Marine Geoscience and Energy Resources 192 (2026) 207810

Contents lists available at ScienceDirect

Marine Geoscience and Energy Resources

journal homepage: www.sciencedirect.com/journal/marine-geoscience-and-energy-resources

Research Paper

Tectono-sedimentary evolution and uplift of the Antalya Basin (Southern Türkiye) during the late Middle Pleistocene: Insights from the Manavgat fan-delta complex

Selma Sarı [a,*], Paola Cipollari [a], Costanza Faranda [a], Süheyla Kanbur [b], Simone Racano [a], Domenico Cosentino [a]

[a] Department of Sciences, Roma Tre University, Rome, Italy
[b] Department of Geological Engineering, Süleyman Demirel University, Isparta, Türkiye

A R T I C L E I N F O

Keywords:
Calcareous nannofossils
Planktonic foraminifera
Surface uplift
Synsedimentary tectonics
Isparta angle
Eastern Mediterranean
Marine isotope stage 7

A B S T R A C T

The Antalya Basin is a late post-orogenic basin formed under extensional and compressional regimes within the Isparta Angle, comprising the Manavgat, Köprüçay, and Aksu sub-basins unconformably overlying the western Taurides. The Manavgat Sub-basin, at the eastern margin of the Antalya Basin, preserves Quaternary fan deltaic successions that record the interplay of tectonics, sediment supply, and sea-level fluctuations. To refine the stratigraphy of the Manavgat Sub-basin and improve our understanding on the tectono-sedimentary evolution of the Antalya Basin, we present new lithostratigraphic and micropaleontological data from a composite section (MNV) of the Manavgat Formation. The MNV composite section records deposition within a deltaic system comprising fan delta front, fan delta front/fan prodelta, and renewed fan delta front facies, reflecting alternating prograding - retrograding cycles. Calcareous nannofossil and planktonic foraminiferal assemblages indicate that the base of the MNV section is younger than ~0.26 Ma (upper Middle Pleistocene) based on the presence of *Emiliania huxleyi*. These biostratigraphic constraints extend the age of marine deposition in the Manavgat Sub-basin into the late Middle Pleistocene, which is significantly younger than previously reported Miocene or Lower Pleistocene marine deposits. This revised regional chronology for the Antalya Basin allow us to interpret a mean uplift rate of ~0.8 m/kyr since the late Middle Pleistocene offering new insights into the tectono-sedimentary evolution at the junction between the southwestern flank of the Central Anatolian Plateau and the Western Anatolian Extensional Province.

1. Introduction

The Tauride orogenic belt in southern Türkiye forms part of the Alpine–Himalayan system (Fig. 1) and preserves a long-lived record of Paleozoic–Cenozoic subduction, collision, and post-orogenic deformation (Okay et al., 2010; Parlak et al., 2019; Schmid et al., 2022). The western and central sectors of this belt converge within the Isparta Angle (IA), which is a transitional zone that links the Hellenic Arc, to the west, with the Cyprus Arc, to the east. The IA represents one of the most structurally complex regions in the Eastern Mediterranean (Blumenthal, 1951; Özgül, 1976; Glover and Robertson, 1998; Deynoux et al., 2005; Kelling et al., 2005; Hall et al., 2014; Över et al., 2016; Nemec et al., 2018).

The Isparta Angle is bounded by the Fethiye-Burdur Fault Zone to the west and the Akşehir Fault Zone to the east (Fig. 1). The Fethiye-Burdur Fault Zone is a major strike-slip fault that extends from the Fethiye Bay to Eğirdir Lake and features transtensional movement (e.g. Koçyiğit et al., 2024; Bozkurt, 2001; Tiryakioğlu et al., 2013; Över et al., 2016). Today, the IA is affected by an extensional tectonic regime, with widespread seismicity along its major active faults (Fig. 2).

The IA recorded alternating extensional and compressional tectonic regimes during the Neogene–Quaternary. Stratigraphic, structural, and paleostress data define three major tectonic phases: 1) pre-Tortonian extensional phase; 2) late Tortonian-Early Pliocene compressional phase; and 3) Late Pliocene-Quaternary extensional phase (e.g., Poisson et al., 2003a, 2003b, 2011; Hall et al., 2014; Koç et al., 2016a, 2016b, 2017; McPhee et al., 2018, 2022; Wasoo et al., 2020).

The first tectonic phase, prior to the Tortonian, corresponds to E–W-

* Corresponding author.
E-mail address: selma.sari@uniroma3.it (S. Sarı).

https://doi.org/10.1016/j.marger.2026.207810
Received 6 February 2026; Received in revised form 30 April 2026; Accepted 3 May 2026
Available online 17 June 2026

directed extension that initiated the Antalya Basin and coeval rifting in the Yalvaç, Altınapa, and Ilgın continental basins (Koç et al., 2016a, 2016b). In the Late Tortonian-Early Messinian, a transition to compressional tectonics produced the Lycian and Aksu deformation phases along the Aksu Thrust. The Lycian phase (~11–7 Ma) generated E–W contraction within the IA core, whereas the Aksu phase (Messinian–Early Pliocene) involved NE–SW to NW–SE shortening and open folding, interpreted to result from gravitational sliding of the Lycian Nappes and/or differential uplift and subsidence across the IA (van Hinsbergen et al., 2010). A third phase began in the Late Pliocene and persists to the present day, characterized by renewed N–S and E-W-directed extension (Glover and Robertson, 1998; Aykut et al., 2023, 2025, 2026), coeval with Middle Pleistocene uplift along the southeastern IA.

The pre-Tortonian extensional phase that affected the IA was responsible for the development of the Antalya Basin, which contains thick Neogene marine clastic and carbonate successions (Flecker et al., 1998, 2005; Karabıyıkoğlu et al., 2000, 2005; Poisson et al., 2003a, 2003b; Deynoux et al., 2005; Çiner et al., 2008). The Antalya Basin has been extensively investigated for its Late Cenozoic evolution, deformation history, and deltaic basin-fill architecture (Akay et al., 1985; Glover and Robertson, 1998; Flecker et al., 1998, 2005; Karabıyıkoğlu et al., 2000, 2005; Poisson et al., 2003a, 2003b; Deynoux et al., 2005).

Recent studies have further refined its stratigraphy, emphasizing the interplay between sediment supply, relative sea-level change, and tectonic activity in controlling deltaic progradation and basin evolution (Sagular and Özer, 2024; Ilgar et al., 2024; Larsen et al., 2024a, 2024b; Wathne et al., 2024; Yılmaz et al., 2024).

Many earlier studies of the Antalya Basin assigned most of the marine deposits to the Miocene (e.g., Flecker, 1995; Glover and Robertson, 1998; Karabıyıkoğlu et al., 2000). Only a few recent studies recognized younger marine deposits within the Antalya Basin. For instance, Sagular and Özer (2024) and Kanbur and Öğretmen (2022) identified Early Pleistocene marine deposits within Manavgat and Aksu sub-basins, respectively, suggesting a more prolonged marine influence in the Antalya Basin than previously thought.

Consequently, the stratigraphy of the Antalya Basin is marked by conflicting age assignments and inconsistent formation boundaries. For example, one of its key successions, the Karpuzçay Formation within the Manavgat Sub-basin, has been variously interpreted as Langhian-Messinian based on planktonic foraminifera dominated by globigerinids (Çiner et al., 2008), Serravallian–Tortonian based on planktonic foraminiferal assemblages, including *Neogloboquadrina acostaensis* (Yılmaz et al., 2024), and Pliocene-Pleistocene based on calcareous nannofossil assemblages, including the *Reticulofenestra pseudoumbilica* Zone (late Early Pliocene) and the *Gephyrocapsa caribbeanica* Subzone (Early Pleistocene) (Sagular and Özer, 2024), reflecting major uncertainties in formation boundaries, depositional environments, and the timing of sedimentation. Such discrepancies likely arise from differences in sampling resolution, sample preparation techniques, and the biostratigraphic analysis method applied. In this type of deposit, characterized by a high degree of reworking, it is necessary to extend the analysis of the nannofossil assemblage to the entire area of the slide, quantifying the percentage of reworking and highlighting the presence of extremely rare primary forms. This prevents an incorrect age assessment. The inconsistencies in the ages reported in the literature have hindered a coherent understanding of the basin's tectono-sedimentary evolution.

We aim to resolve these discrepancies by demonstrating, with a multi-proxy dataset, that the Antalya Basin hosted marine depositional environments at least until the late Middle Pleistocene (late Chibanian), considerably younger than previously inferred. The exposed fan-delta succession of the Quaternary Manavgat Formation, in the Manavgat Sub-basin, provides an exceptional record for reconstructing its tectono-sedimentary evolution, close to the end of marine deposition in the Antalya Basin, before uplift of the region drove marine regression.

Through integrated facies and micropaleontological analyses, we intend to (i) refine the Quaternary stratigraphy, facies architecture, and

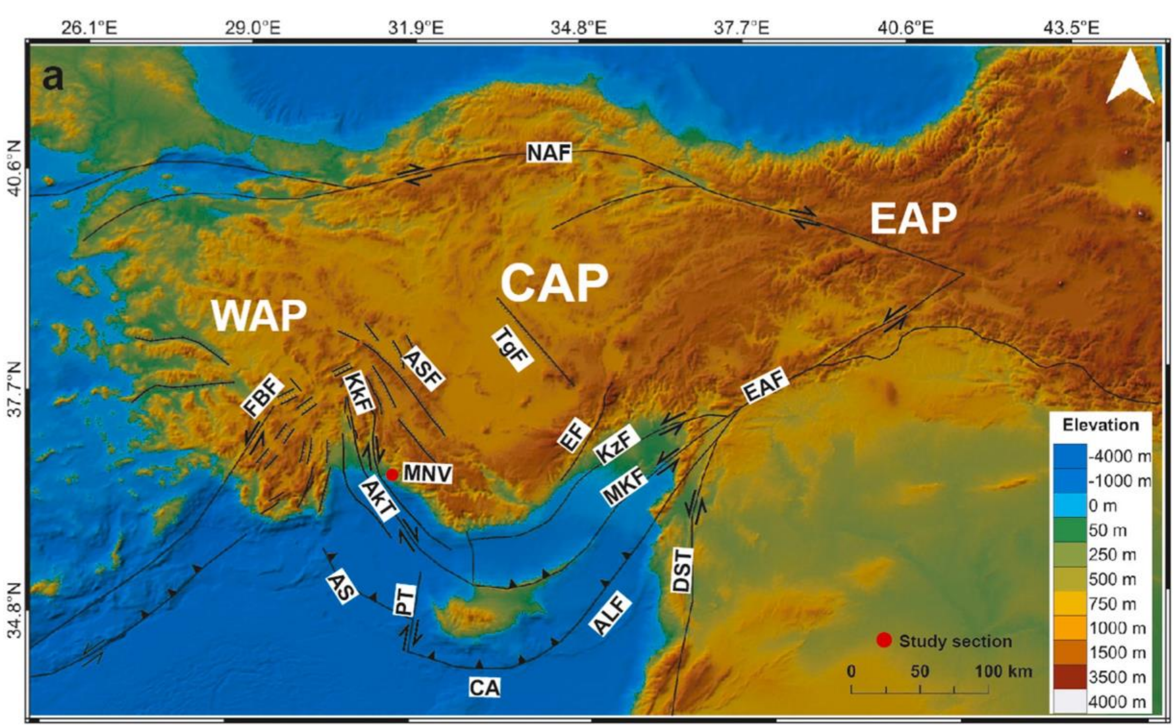

Fig. 1. Simplified regional topography and tectonic map of Anatolia showing the location of the studied section (MNV) within the Isparta Angle. CAP, Central Anatolian Plateau; EAP, Eastern Anatolian Plateau; WAP, Western Anatolian Province; NAF, North Anatolian Fault; EAF, East Anatolian Fault; DST, Death Sea Transform Fault; CA, Cyprus Arc; PT, Paphos Transform; AS, Antalya Slab; ALF, Amos-Larnaka Fault; AkT, Aksu Thrust; KkF, Kırkkavak Fault; EF, Ecemiş Fault; KzF, Kozan Fault; MKF, Misis-Kyrenia Fault; TgF, Tuz Gölü Fault, FBF Fethiye-Burdur Fault; ASF, Akşehir Fault.

depositional history of the sub-basin; (ii) establish a revised chronostratigraphic framework based on calcareous nannofossil and foraminiferal assemblages; (iii) quantify the timing and rate of post-depositional uplift; and (iv) propose geodynamic mechanisms that may explain the tectono-sedimentary evolution of the sub-basin.

Collectively, our results improve our understanding of the late Quaternary tectono-sedimentary evolution of the Antalya Basin and the broader IA, and they provide new constraints on the geodynamics of the Eastern Mediterranean.

1.1. Geological setting and stratigraphy

The southwestern margin of the CAP is underlain by Mesozoic autochthonous carbonates of the Geyikdağı Unit (Özgül, 1976; Akay and Uysal, 1988; Schmid et al., 2022). This unit is tectonically overlain by the allochthonous Beyşehir-Hoyran, Antalya, and Alanya nappes, which consist of ophiolitic mélanges, metamorphic rocks, platform carbonates, and Eocene carbonate–clastic sequences (Özgül, 1976; Şengör and Yılmaz, 1981). The Antalya Basin developed unconformably atop these nappes, within the IA, during the Late Cenozoic.

The Antalya Basin is bounded by two major fault zones: the Fethiye-Burdur Fault Zone, to the west, and the Sultandağı-Akşehir Fault Zone, to the east (Fig. 2). Within the Antalya Basin, the activity of other tectonic structures, such as the N–S-trending Kırkkavak Fault (KkF) and the W- to SW-verging Aksu Thrust (AkT), have led to its division into three sub-basins (Fig. 2): Aksu, Köprüçay, and Manavgat (Dumont and Kerey, 1975; Akay et al., 1985; Monod et al., 2006; Çiner et al., 2008; Poisson et al., 2011; Hall et al., 2014). The Kırkkavak Fault, originally a paleotectonic structure, was reactivated as a normal fault during the Quaternary, reflecting a regional transition to extensional tectonics linked to southward retreat of the subducting Neo-Tethyan slab (Doğan et al., 2017; Koçyiğit et al., 2024; Aykut et al., 2023, 2025, 2026).

The stratigraphy of the Manavgat Sub-basin has been documented in detail by numerous studies, and a total of eight main formations have been recognized, spanning from the Early Miocene to the Quaternary (Fig. 3). The lowermost unit, the Tepekli Formation (Burdigalian), consists predominantly of alluvial-fan and fan-delta conglomerates (Karabıyıkoğlu et al., 2000; Çiner et al., 2008). It is overlain by the Oymapınar Formation (Upper Burdigalian–Langhian), which is composed of reefal limestones (Flecker et al., 1998; Karabıyıkoğlu et al.,

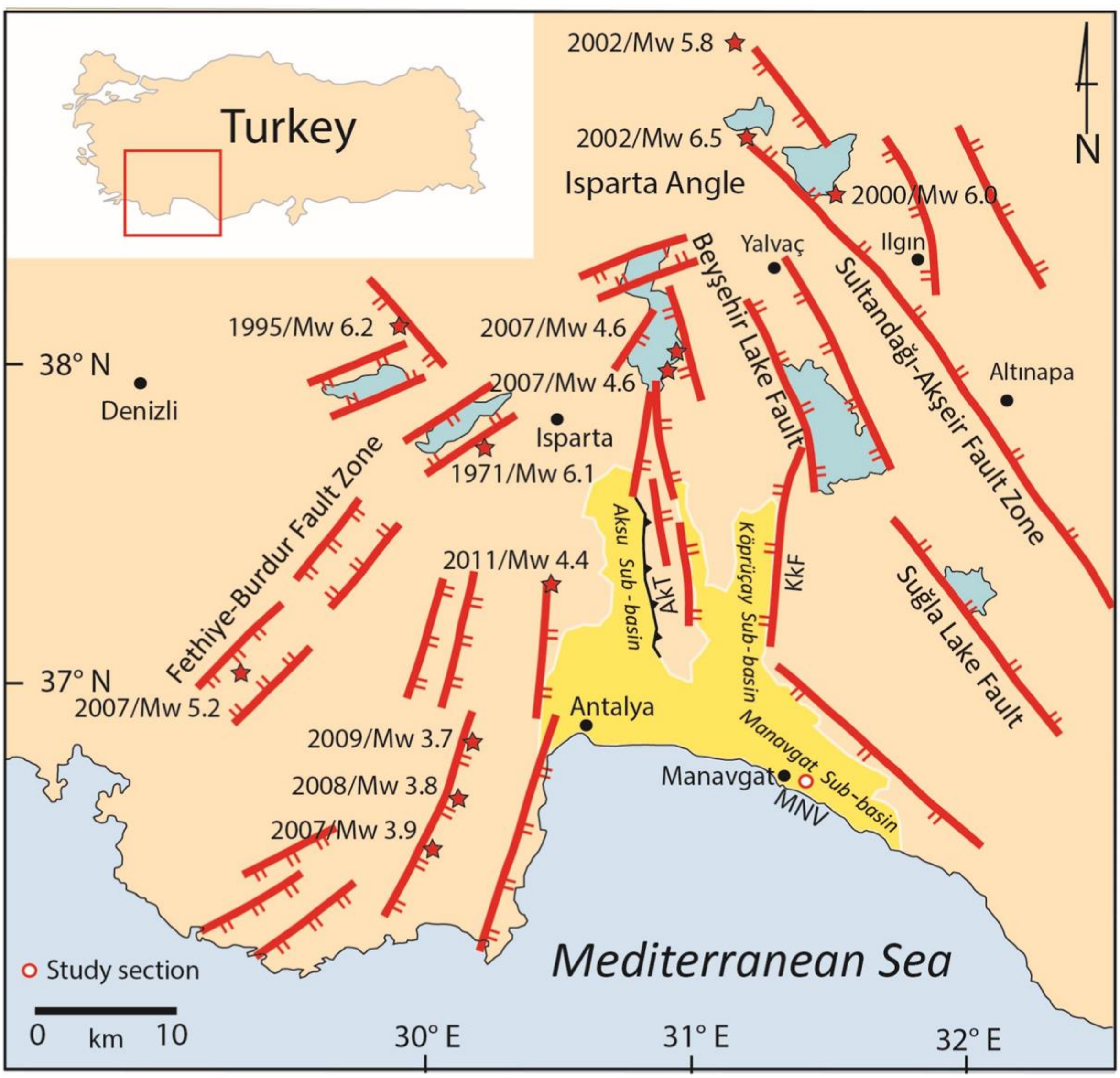

Fig. 2. Seismotectonic setting of the Isparta Angle, Eastern Mediterranean region (modified from Över et al., 2016), showing the extension of the Neogene Antalya Basin (in yellow) and relative sub-basins (Aksu, Köprüçay, and Manavgat). Red stars indicate location and year of earthquakes with Mw > 3.5. KkF – Kırkkavak Fault; AkT – Aksu Thrust. (For interpretation of the references to colour in this figure legend, the reader is referred to the Web version of this article.)

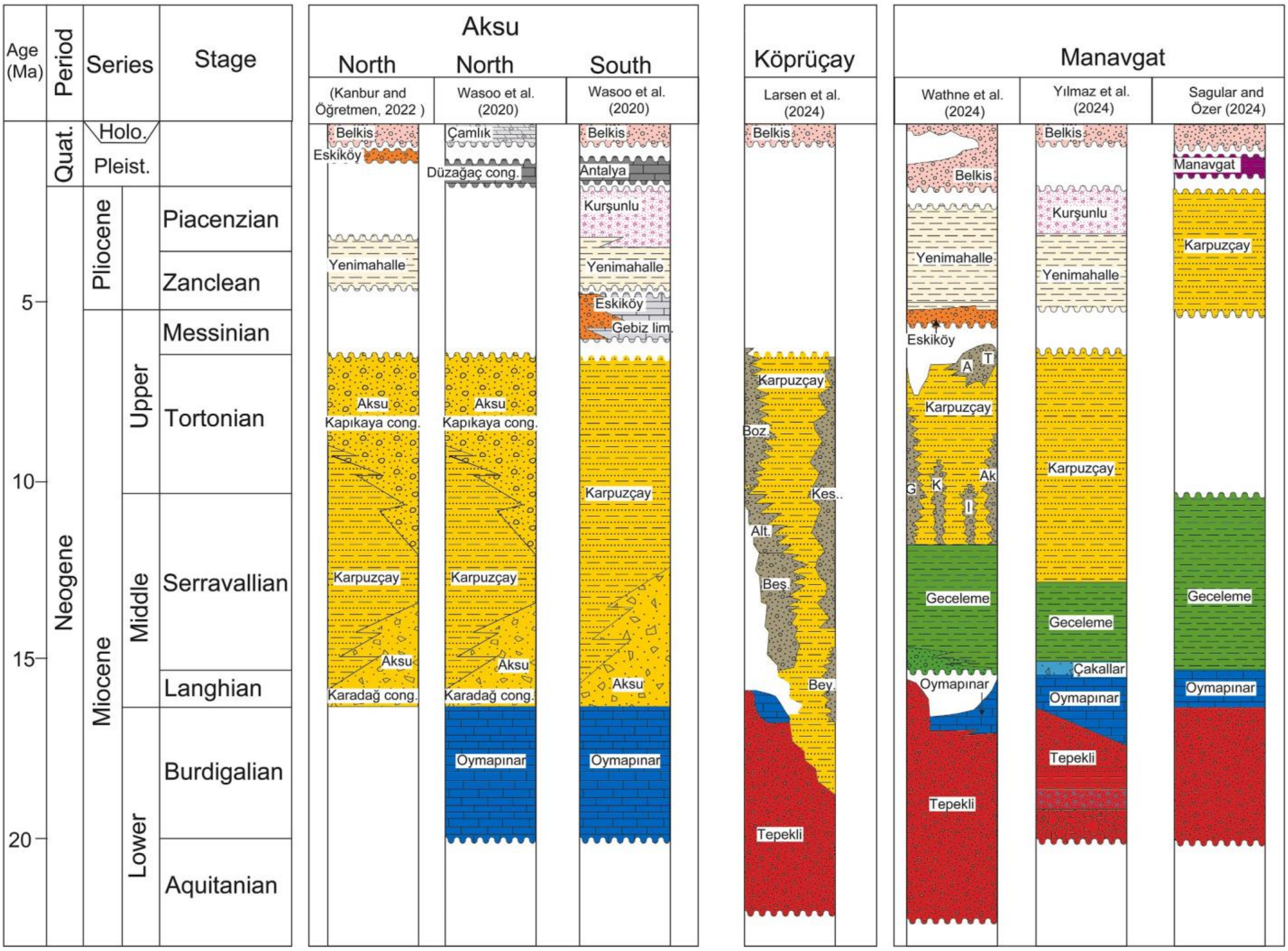

Fig. 3. Lithostratigraphic framework of three major sub-basins of the Antalya Basin (Aksu, Köprüçay, and Manavgat) during the Neogene–Quaternary. The figure summarizes the documented stratigraphic units, their age assignments, and the major depositional systems recorded across the basin. Delta complexes are labelled using the following abbreviations: Beydiğin (Bey), Altınkaya (Al), Beşkonak (Bes), Bozburun (Boz), Kesme (Kes), Göktaş (G), Katırnemeği (K), İhtiyarlı (I), Akseki (Ak), and Taşlık (T), Asar (A).

2000; İslamoglu, 2002; Çiner et al., 2008). Above this, the Çakallar Formation (Langhian) comprises fore-reef talus deposits (Akay et al., 1985). The overlying Geceleme Formation (Upper Langhian–Serravallian) consists of grey claystone and marl rich in planktonic foraminifers, interbedded with thin sandstone layers (Akay et al., 1985; Karabıyıkoğlu et al., 2000; İslamoglu, 2002; Çiner et al., 2008). The Karpuzçay Formation (Serravallian-Tortonian) conformably overlies the Geceleme Formation and is characterized by alternating mudstone, siltstone, sandstone, and conglomerate (Akay et al., 1985; Çiner et al., 2008; Karabıyıkoğlu et al., 2000; Yılmaz et al., 2024). The Yenimahalle and Kurşunlu formations (Pliocene) consists of alternating limestone–claystone–sandstone and conglomerate–sandstone–mudstone successions, respectively (Yılmaz et al., 2024).

In the Manavgat Sub-basin (Fig. 4), in contrast to these previous attributions, Sagular and Özer (2024) consider the lower part of the Karpuzçay Formation to be Zanclean in age, due to the occurrence of calcareous nannofossils attributable to the *Reticulofenestra pseudoumbilica* zone (NN15, late Early Pliocene), while defining a new formation (Manavgat Formation) to indicate the youngest portion of the Karpuzçay Formation, in which they recognized calcareous nannofossils attributable to the *Gephyrocapsa caribbeanica* subzone (NN19a, Early Pleistocene). The Manavgat Formation is composed of shallow marine and coastal clastic deposits (Sagular and Özer, 2024). The overlying Belkıs Formation (Quaternary) consists of fluvial conglomerates exposed mainly along the southern parts of the basin, near the present-day coastline (Yılmaz et al., 2024).

In comparing the different proposed stratigraphies for the Antalya Basin (Fig. 3), the main difference that emerges is the temporal attribution of formations such as the Karpuzçay Formation (Sagular and Özer, 2024) and the Eskiköy Formation (Kanbur and Öğretmen, 2022). These new age assignments derive from the discovery of planktonic foraminifera and calcareous nannofossils referable to biozones that are much younger than previously thought for the same formations (e.g., Akay et al., 1985; Çiner et al., 2008; Karabıyıkoğlu et al., 2000; Yılmaz et al., 2024). These new findings significantly change the previously inferred age of the marine deposits and call into question the chronology of the tectono-sedimentary evolution as proposed by previous various authors.

2. Material and methods

Our present study focuses on the analysis of three stratigraphic sections, which we here combined into one composite, located in the Manavgat Sub-basin near the Uzunlar neighbourhood of Antalya, southwestern Türkiye. According to previous studies on the Manavgat Sub-basin, our composite section should fall within the Karpuzçay Formation (Serravallian-Tortonian; Akay et al., 1985; Çiner et al., 2008; Karabıyıkoğlu et al., 2000; Yılmaz et al., 2024) and should contain the

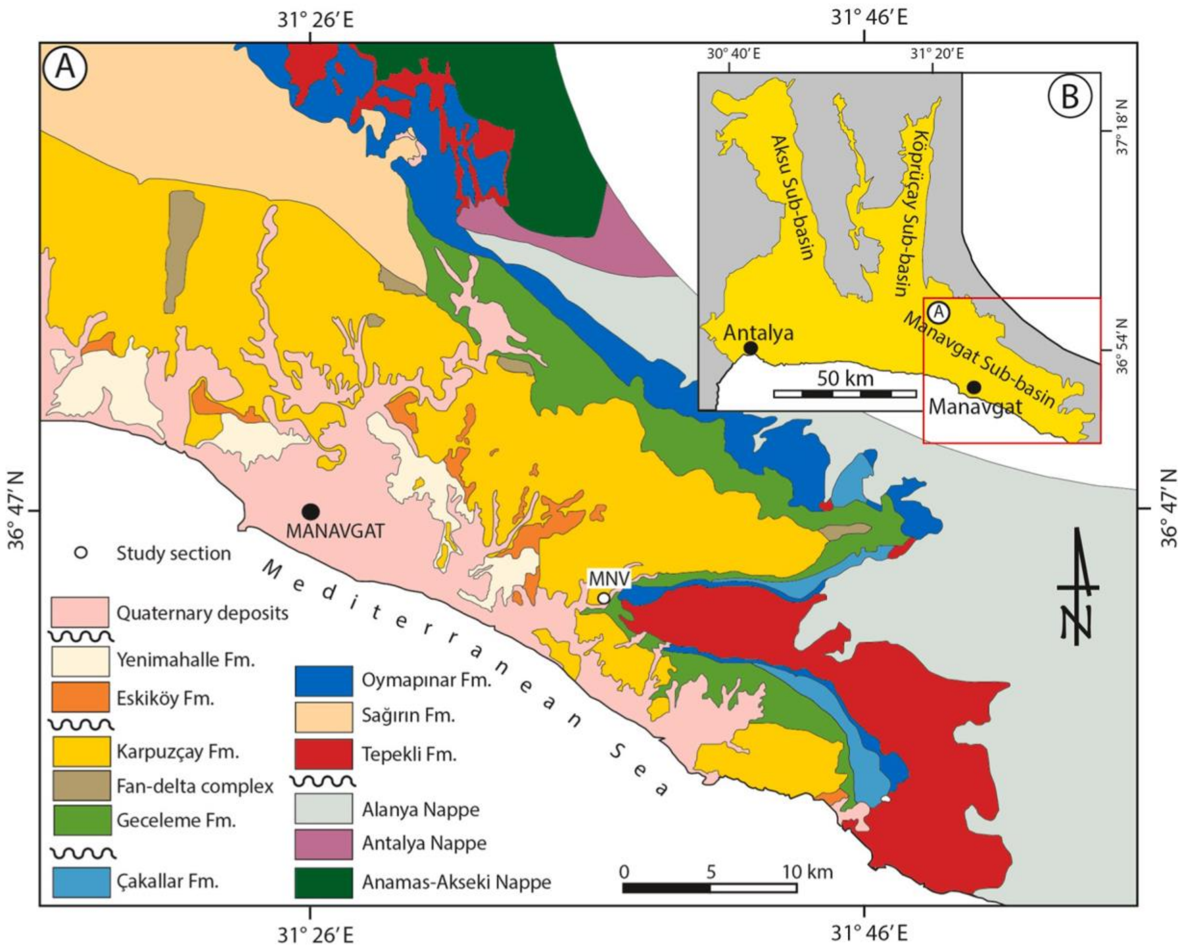

Fig. 4. (A) Geological map of the Manavgat Sub-basin (modified after Wathne et al., 2024) showing Neogene and Quaternary sedimentary units, with locations of the studied composite sections (MNV). (B) Simplified geological map of the Antalya Basin, showing its three sub-basins, in yellow, and the bedrock successions, in grey. The red rectangle shows the position of Fig. 4A within the Antalya Basin. (For interpretation of the references to colour in this figure legend, the reader is referred to the Web version of this article.)

boundary between the Karpuzçay Formation (Lower Pliocene) and the Manavgat Formation (Lower Pleistocene) according to the stratigraphic arrangement proposed by Sagular and O ̈zer (2024) for the Manavgat Sub-basin.

The composite section integrates two continuous successions: MNV4 and MNV1–2 sections (Fig. 5). The MNV4 section (36°44′28.74″N, 31°37′21.07″E, base of section; 36°44′18.84″N; 31°36′52.87″E, top of section) is approximately 65 m thick and exposed at ~50 m above Mean Sea Level (MSL). It is stratigraphically overlain by the MNV1–2 succession (36°44′30.76"N, 31°36′50.77″E, base of section; 36°44′38.20"N; 31°37′6.03″E, top of section), which comprises an additional 35 m of strata. The top of the MNV2 interval reaches ~143 m above MSL, and with an estimated covered gap of ~25 m between the MNV4 and MNV1-2 measured sections.

Based on lithological correlation, stratigraphic position, and lateral continuity, the MNV4 and MNV1–2 successions are interpreted as a single depositional sequence forming the MNV composite section. Marl layers were systematically sampled throughout the MNV composite section for the micropaleontological analyses. A total of 46 samples were collected, 25 from MNV4, 9 from MNV1, and 12 from MNV2.

To establish the chronological framework of the composite succession, semi-quantitative analyses of calcareous nannofossils were performed using a concentrated preparation method (De Capoa et al., 2003). As the concentration procedure markedly increases the number of specimens per field of view, typically ~ ten times higher than in standard smear-slide preparations, a reduced number of fields is sufficient to capture the full assemblage.

Accordingly, two counting strategies were applied. For the general assemblage, ten representative fields of view were examined per slide, which provided a stable estimate of species abundances due to the high specimen density of the concentrated preparations. In contrast, to ensure that even the rarest forms of the assemblages are sampled (like *Emiliania huxleyi*) approximately 350 fields of view were scanned. Specimen frequencies were recorded as the number of individuals per mm^2. Biostratigraphic interpretations and age determinations were based on the standard Mediterranean calcareous nannofossil zonation of Di Stefano et al. (2023).

Qualitative foraminiferal biostratigraphic analyses were conducted to complement the nannofossil data and with planktonic assemblages used to refine the age model and benthic assemblages providing constraints on palaeobathymetric conditions. All samples were wet-sieved through a 63-μm mesh using tap water, without any prior acid treatment, and residues were dried at room temperature. Sample preparation, identification of the species, and photographing some species were performed at the Süleyman Demirel University (SDU), Department of Geological Engineering and at SDU, Innovative Technologies Application and Research Centre facilities. The biostratigraphic interpretation and age determinations were based on comparison with the standard Mediterranean foraminiferal biostratigraphic zonation proposed by Lirer et al. (2019).

Although the same preparation procedure was applied to recover ostracods for paleobathymetric analysis, no ostracod specimens were

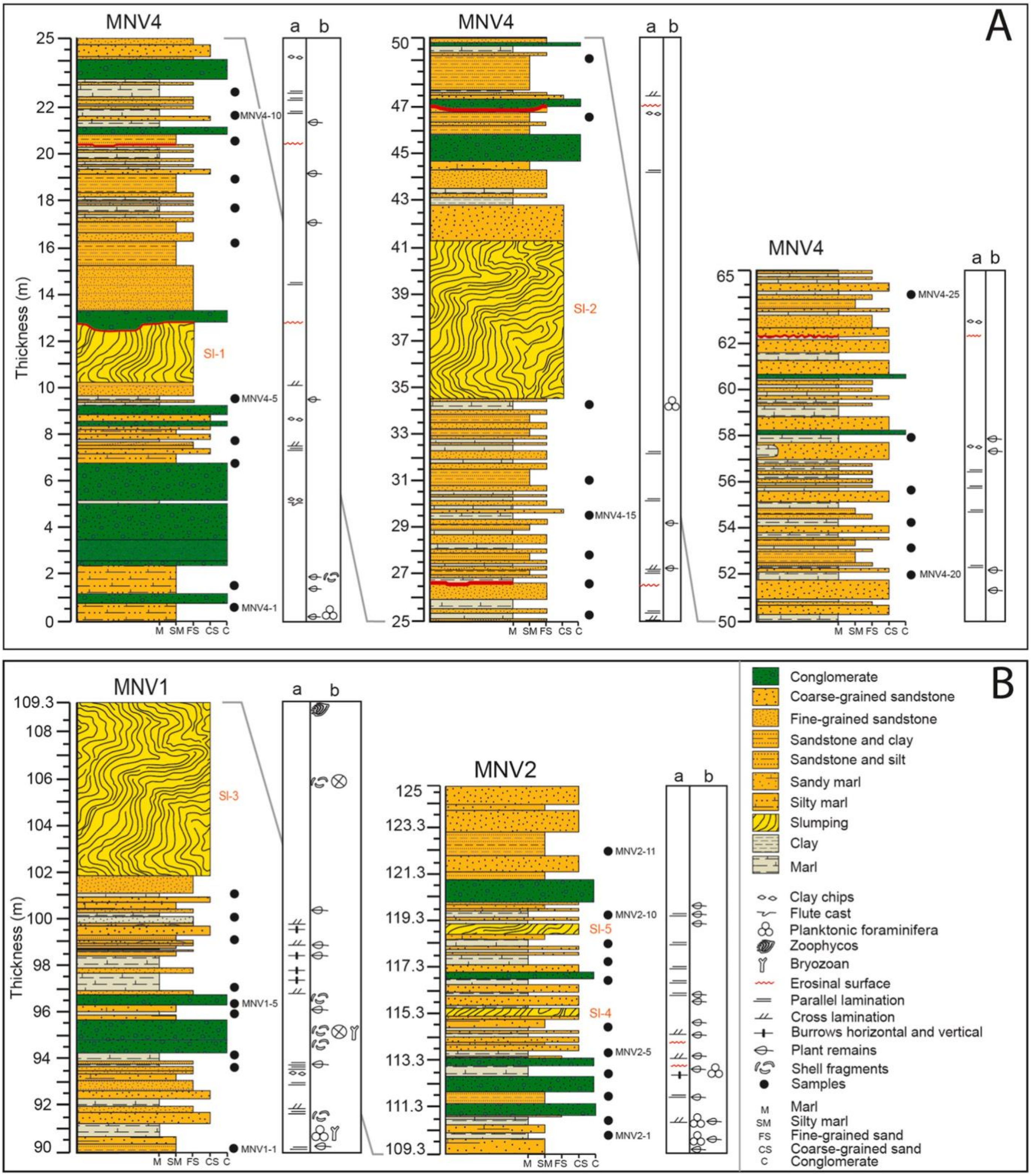

Fig. 5. (A) Detailed lithostratigraphic log of the MNV4 section (0-65 m of MNV composite section). (B) Detailed lithostratigraphic log of the MNV1-2 composite section (90-125 m of MNV composite section). Panels a and b report field observations on sedimentary structures and fossil components, respectively; the panel on the right shows the legend for detailed lithological, sedimentological, and fossil content symbols for both sections.

recovered from any of the samples.

3. Results

3.1. Lithostratigraphy of the MNV composite section

The MNV composite section is approximately 125 m thick, encompassing the integrated MNV4, MNV1 and MNV2 sections (Figs. 5 and 6). It exhibits a rhythmic alternation of marl, silty marl, fine-to coarse-grained sandstone, and conglomerate, interbedded with slumped horizons and soft-sediment deformation structures.

3.1.1. MNV4 section

The basal part (0–2.4 m; base of MNV4) consists predominantly of silty marls and includes a thin, distinct matrix-supported conglomerate bed with decimetric thickness and clast sizes ranging from millimetres to centimetres (Fig. 5A and 6F). The 2.4-13.4 m interval is dominated by clast-supported conglomerates with mm-to cm-sized clasts, a poorly sorted medium-grained sandstone matrix (~30% of the unit), and interbedded coarse-grained sandstones with crude lamination, parallel to wavy ripple bedded fine grained sandstone (Fig. 6D), medium-grained sandstones with clay chips and sole marks, and silty marls. A 2.5-m-thick intraformational slump horizon (Sl-1) occurs within this interval (Fig. 6E). It shows an erosional basal surface and is composed of chaotically deformed marls and carbonate pebbles.

Between 13.4 and 20.9 m, the succession consists mainly of finely laminated sandstones and clays, interbedded with thin marly layers. This interval is overlain by coarse-grained sandstones and clast-supported conglomerates (20.9–24.7 m), which are poorly to moderately sorted and contain ~25% of sandy matrix. From 24.7 to 44.7 m, the section alternates between fine-grained sandstones exhibiting parallel and cross-lamination, crudely laminated coarse-grained sandstones, and marls (Fig. 6C). A second major intraformational slump (Sl-2) occurs in the upper part of this interval (~7 m thick), consisting of chaotically deformed marls and pebbles, with shell fragments, sparse *bryozoa*n colonies, and fragments of coral colonies (Fig. 6B). Between 44.7 and 47.5 m, deposits are dominated by clast-supported conglomerates interbedded with fine-to coarse-grained sandstones; the conglomerates display channel-like basal erosional surfaces. The uppermost part of the MNV4 section (47.5–65 m) consists of alternating fine-to coarse-grained sandstones, minor matrix-supported conglomerates (poorly sorted, mm–cm clasts), and marls (Fig. 6A).

3.1.2. MNV1 and MNV2 sections

The MNV1–2 succession (Fig. 5B), which overlies the MNV4 section after an estimated ~25 m of covered and unmeasured section, spans from 90 to 125 m in the composite log. The lower interval (90–94.25 m; MNV1) is composed mainly of marls and silty sandstones, and fine-to

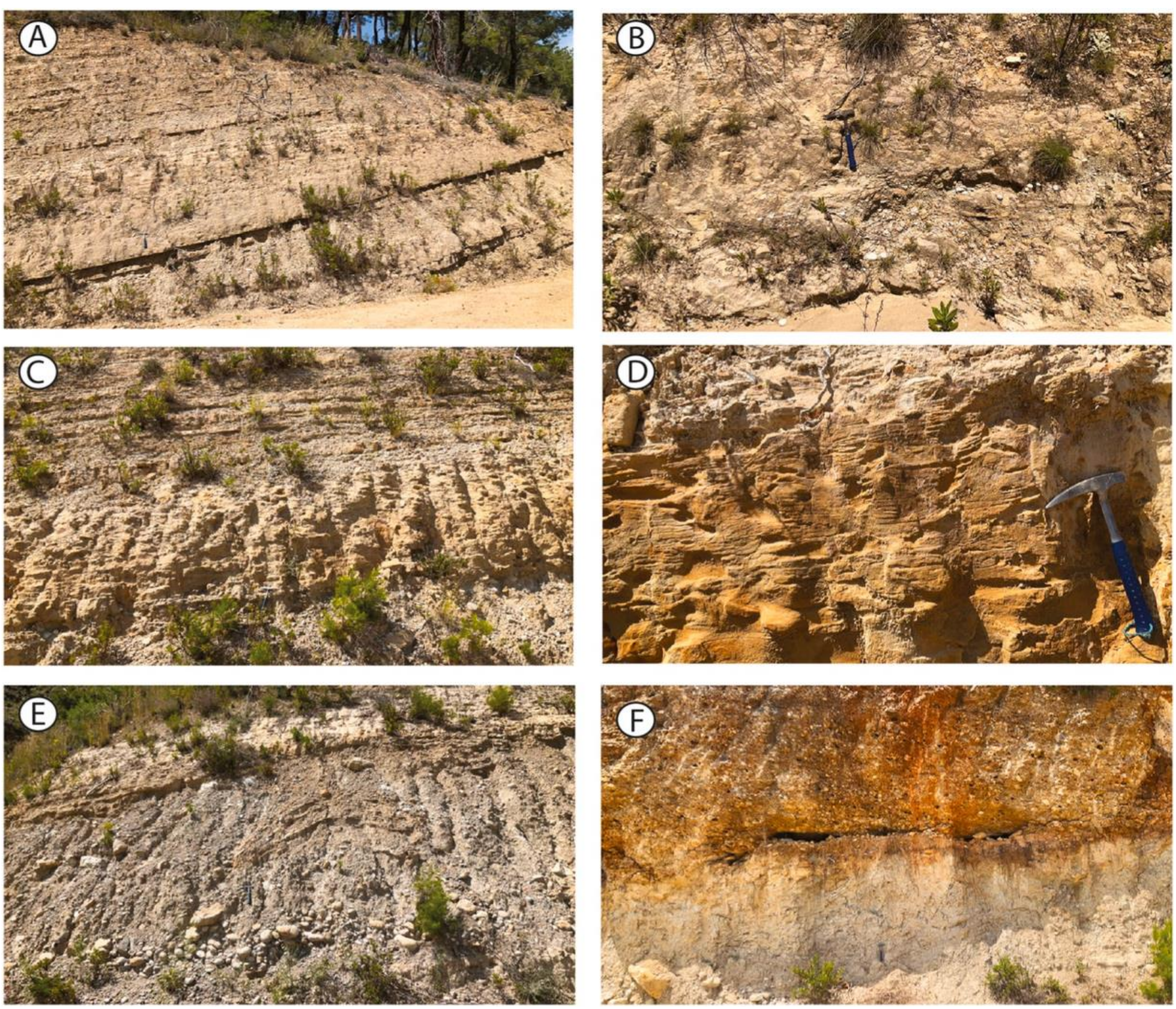

Fig. 6. Field photographs showing representative physical sedimentary structures from top to bottom of the MNV4 section. (A) well-bedded alternations of marls and fine-to coarse-grained sandstones from the uppermost part of the section; (B) 7-m-thick slumped horizon (SL-2) from the middle portion of the section; (C) well-bedded alternation of conglomerates and coarse-to fine-grained sandstones from the lower part of the measured section; (D) parallel to wavy ripple bedded fine grained sandstone from the lower part of the measured section; (E) 2.5-m-thick slumped horizon (SL-1) from the lower part of the section; (F) lowermost portion of the section showing a disrupted marl horizon overlaid by a thick conglomerate bed.

medium-grained sandstones with parallel and cross-lamination (Fig. 7H). This interval fines upward and is overlain by a clast-supported conglomerate (94.25–96.8 m) with a channel-like erosional base. Between 96.8 and 108.1 m, the succession is dominated by marls and silty marls, interbedded with fine-to medium-grained sandstones showing parallel and cross-lamination; brown to black organic-rich laminae are common, particularly between 96.8 and 101 m (Fig. 7D-F-G). This interval contains the third major slump horizon, Sl-3 (~7.5 m thick; Fig. 7A-B-C), composed of chaotic deposits formed of marls with oxidised horizons, sand, and conglomerate, with abundant shell fragments, bryozoans, and fragments of coral colonies. (Fig. 7C). In the MNV1 section, medium-to fine-grained sandstones with cross and parallel laminations are present.

The MNV2 section (109.3–125 m) continues above the Sl-3 intraformational slumped horizon of MNV1. The 110.9–117 m interval is dominated by clast-supported conglomerates with a sandy matrix, interbedded with marls and silty sandstones, and fine-to medium-grained sandstones with crude parallel- and cross-lamination

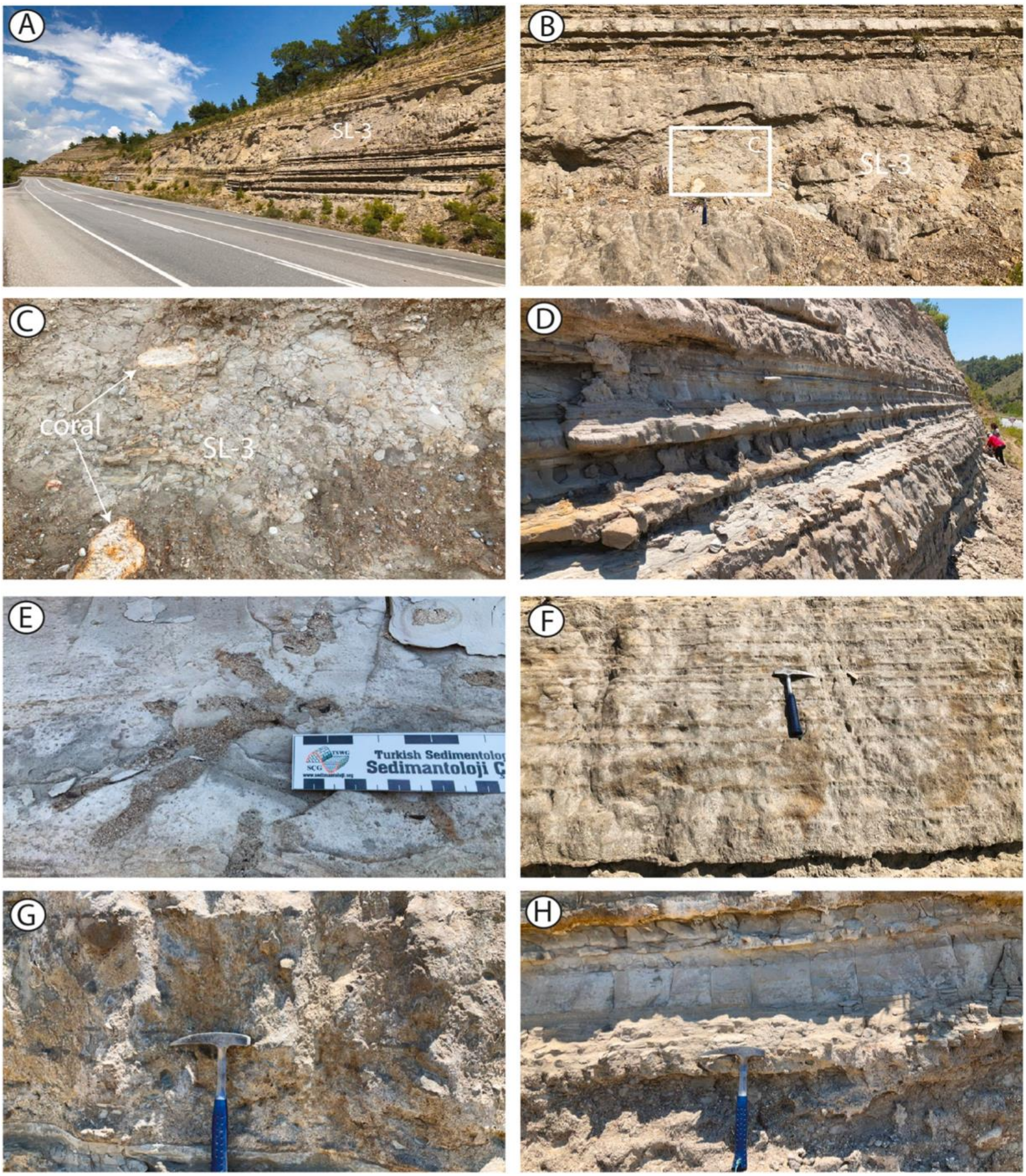

Fig. 7. Field photographs showing representative physical sedimentary structures (from top to bottom) of the MNV1-2 composite section. (A) Panoramic view of the MNV1-2 composite section, along the D695 road (Manavgat-Konya road), showing the SL-3 slumped horizon; (B) topmost part of the SL-3 slumped horizon; (C) close-up of the SL-3 slumped horizon (see box in B) showing a muddy-supported conglomerate with fragments of coral colonies; (D) middle part of the MNV1 section showing well-bedded succession of marls, sandy marls, fine- and coarse-grained sandstones; (E) bioturbation (*Thalassinoides* sp.) in a marly horizon from the middle part of the MNV1 section; (F) coarse-to fine-grained sandstone bed from the lower part of the MNV1 section showing well-developed parallel-lamination; (G) sandy marl bed rich in clay chips from the lowermost part of the MNV1 section; (H) well-bedded lowermost portion of the MNV1 section showing alternations of marls, sandy marls, fine- and coarse-grained sandstones, and conglomerates.

(Fig. 7A–B). The uppermost unit (117–125 m) consists of thick, coarse-grained sandstones with crude laminations, marking the top of the MNV composite section. Within MNV2, two thin intraformational slump layers (~0.5 m each) occur, composed of chaotic marls, sand, and pebble mixtures (Sl-4 and Sl-5; Fig. 5B).

Throughout the MNV composite section, marls are rich in planktonic foraminifera and, secondarily, benthonic foraminifera. Bioturbation structures are widespread, including *Zoophycos* sp., *Thalassinoides* sp., and *Planolites* sp. (Fig. 7E).

3.2. Micropaleontological results

3.2.1. Calcareous nannofossils

Calcareous nannofossil assemblages from the MNV composite section are dominated by long-range and reworked taxa, whereas biostratigraphically significant species are rare (Figs. 8 and 9). The most

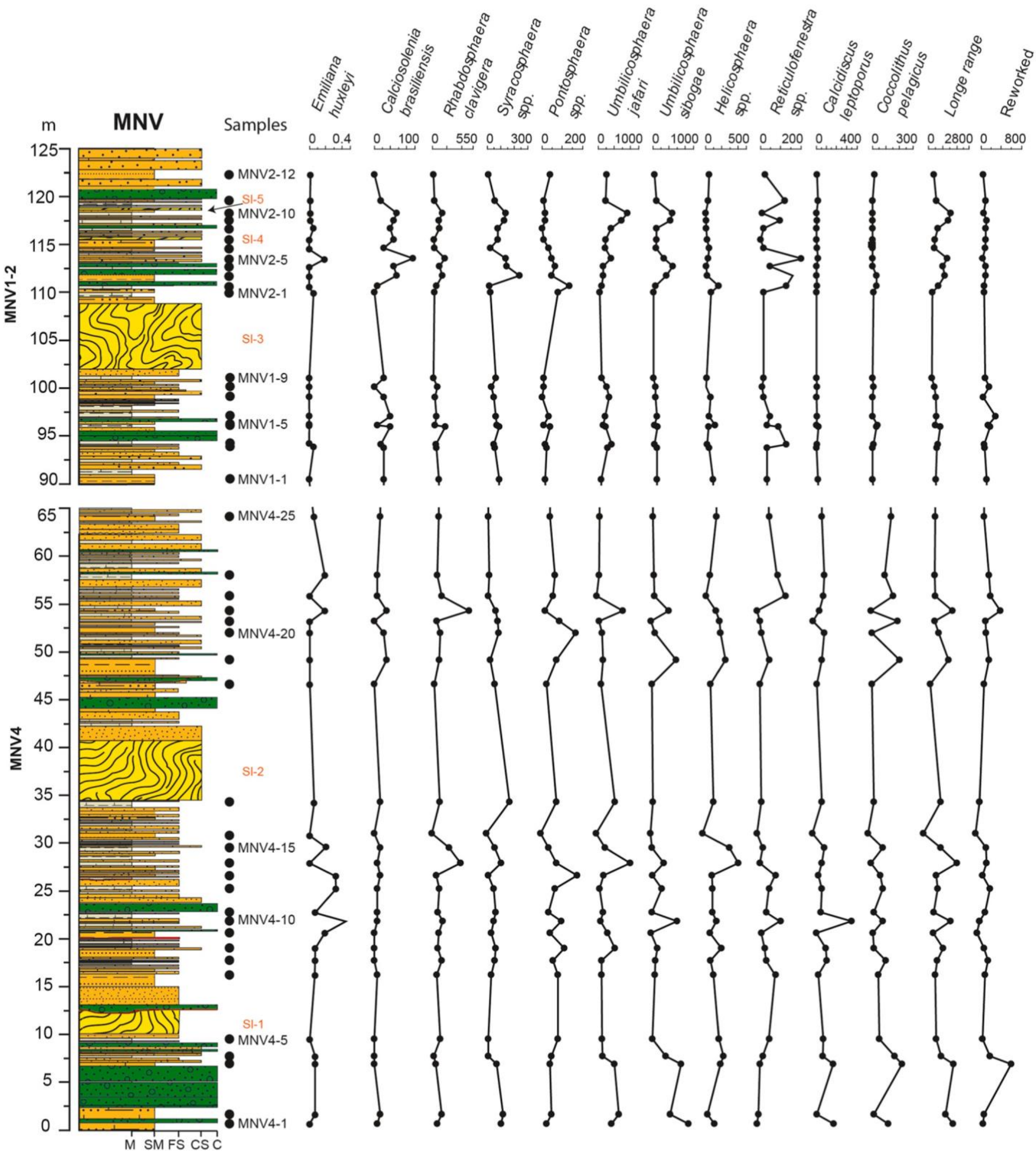

Fig. 8. Quantitative calcareous nannofossil biostratigraphy at MNV composite section. Abundances are expressed as number of specimens per mm^2.

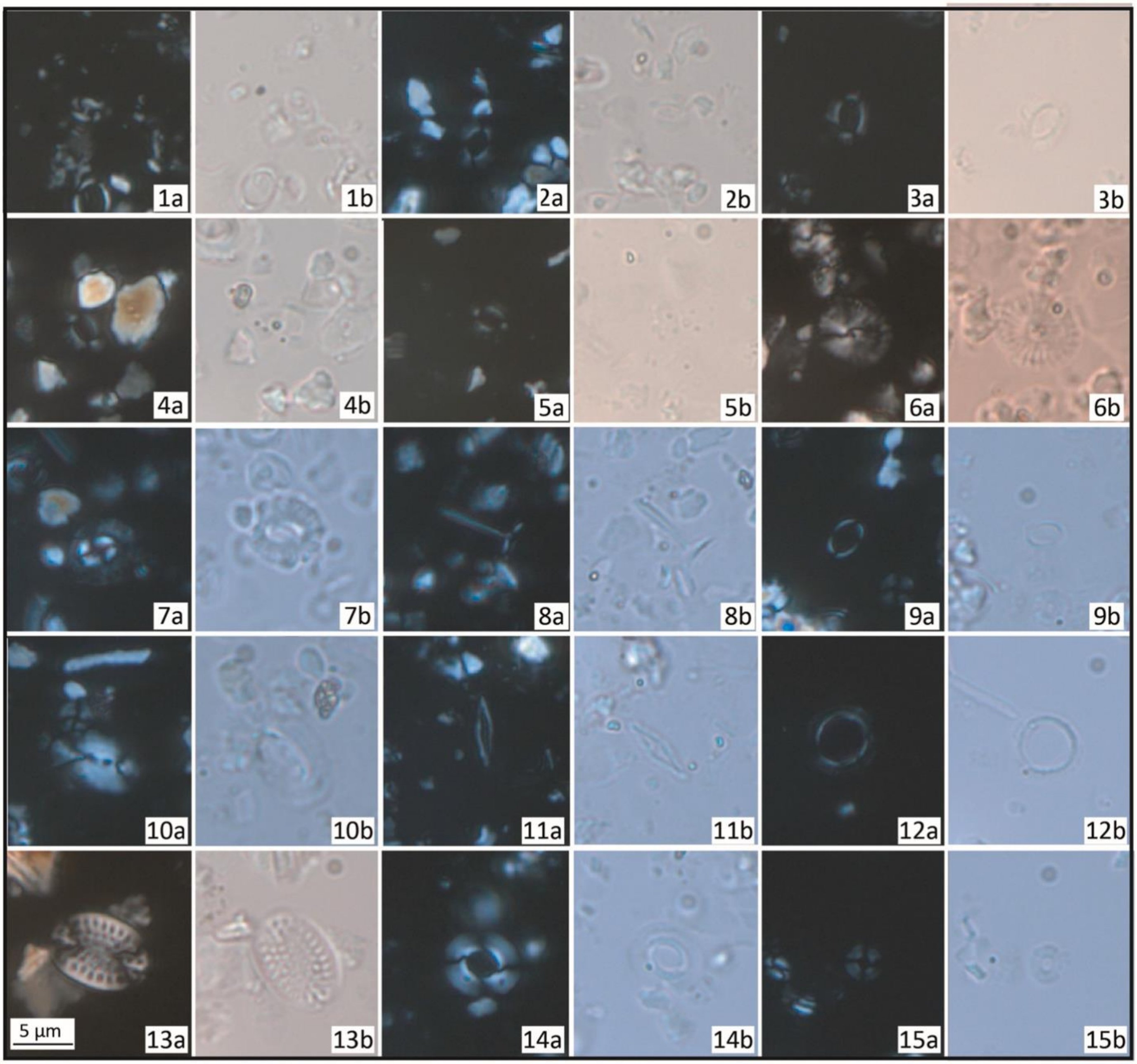

Fig. 9. Microphotographs of calcareous nannofossils from studied sections. (1) small *Gephyrocapsa* (MNV2-2); (2-5) *Emiliania huxleyi* (MNV4-15, MNV4-7, MNV4-11, MNV2-8); (6) *Calcidiscus leptoporus* (MNV4-10); (7) *Coccolithus pelagicus* (MNV4-1); (8) *Rhabdosphaera clavigera* (MNV1-8); (9) *Syracosphaera spp.* (MNV4-12); (10) *Helicosphaera* carteri (MNV1-18); (11) *Calciosolenia sp.* (MNV1-1); (12) *Umbilicosphaera sibogae* (MNV2-5); (13) *Pontosphaera carteri*, (MNV4-11); (14) *Reticulofenestra* sp. (MNV1-4); (15) *Umbilicosphaera jafari* (MNV4-10). (a) Crossed nicols; (b) Parallel nicols. Scale bar uniform for all images.

common taxa include *Coccolithus pelagicus, Umbilicosphaera jafari, U. sibogae, Helicosphaera* spp., *Calcidiscus leptoporus, Pontosphaera* spp., *Syracosphaera* spp., *Calciosolenia* sp., and *Rhabdosphaera clavigera* (Fig. 8). Small *Gephyrocapsa* specimens occur sporadically, while medium-sized *Gephyrocapsa* were not observed. Importantly, *Emiliania huxleyi* was identified throughout both MNV4 and MNV1-2 sections, although in low abundance. The first occurrence (FO) of *E. huxleyi* is dated to approximately 0.26 Ma in the Mediterranean region (Di Stefano et al., 2023), marking a key biostratigraphic boundary within the Middle Pleistocene. Therefore, its consistent presence within the studied sections indicates that deposition of the MNV composite section took place after ~0.26 Ma**,** placing the sedimentation of both sections in the late Middle Pleistocene**.**

Long-range and reworked species display similar vertical distribution patterns throughout the section, suggesting significant reworking. These include specimens of *Sphenolithus spp., Discoaster spp., Blackites sp., Pontosphera spp., Reticulofenestra umbilicus, Braarudosphaera sp.,* and *Pseudoemiliania lacunosa*, many of which are characteristic of older Neogene assemblages and are therefore interpreted as reworked within the studied succession. In the MNV1 and MNV2 sections the relative abundance of reworked taxa decreases, contrasting with an increase in sedimentation rate. This pattern can be explained by considering that also many long-ranging species are reworked, since they increase during the same stratigraphic interval (Fig. 8).

3.2.2. Foraminifera

The planktonic foraminiferal assemblage in the MNV composite section includes several stratigraphically significant species occurring during the Pleistocene (Fig. 10). *Globoturborotalita rubescens* and *Neogloboquadrina* spp. sx are found frequently throughout the entire section, and to a lesser extent, *Globigerinella calida* is also found frequently. *Globigerinoides ruber* (pink) is frequently present throughout the MNV4 section and sporadically appears in MNV 1 and MNV2 sections. *Globoconella inflata* is encountered only at the bottom of the MNV1 section, whereas *Globorotalia crassaformis*, *G. truncatulinoides*, and *G. tenellus* are found sporadically in a limited number of samples. An important Pleistocene marker species is the benthic foraminifera *Hyalinea balthica*, which is also found rarely in the MNV4 and MNV1 sections (Figs. 10 and 11). Its occurrence is consistent with outer shelf to upper slope (circalittoral) environments, typically associated with relatively well-oxygenated bottom waters and moderate organic matter supply (Drinia et al., 2014).

4. Discussion

4.1. Depositional environments and facies evolution

Based on lithological and sedimentological characteristics, two distinct facies associations are recognized along the MNV composite

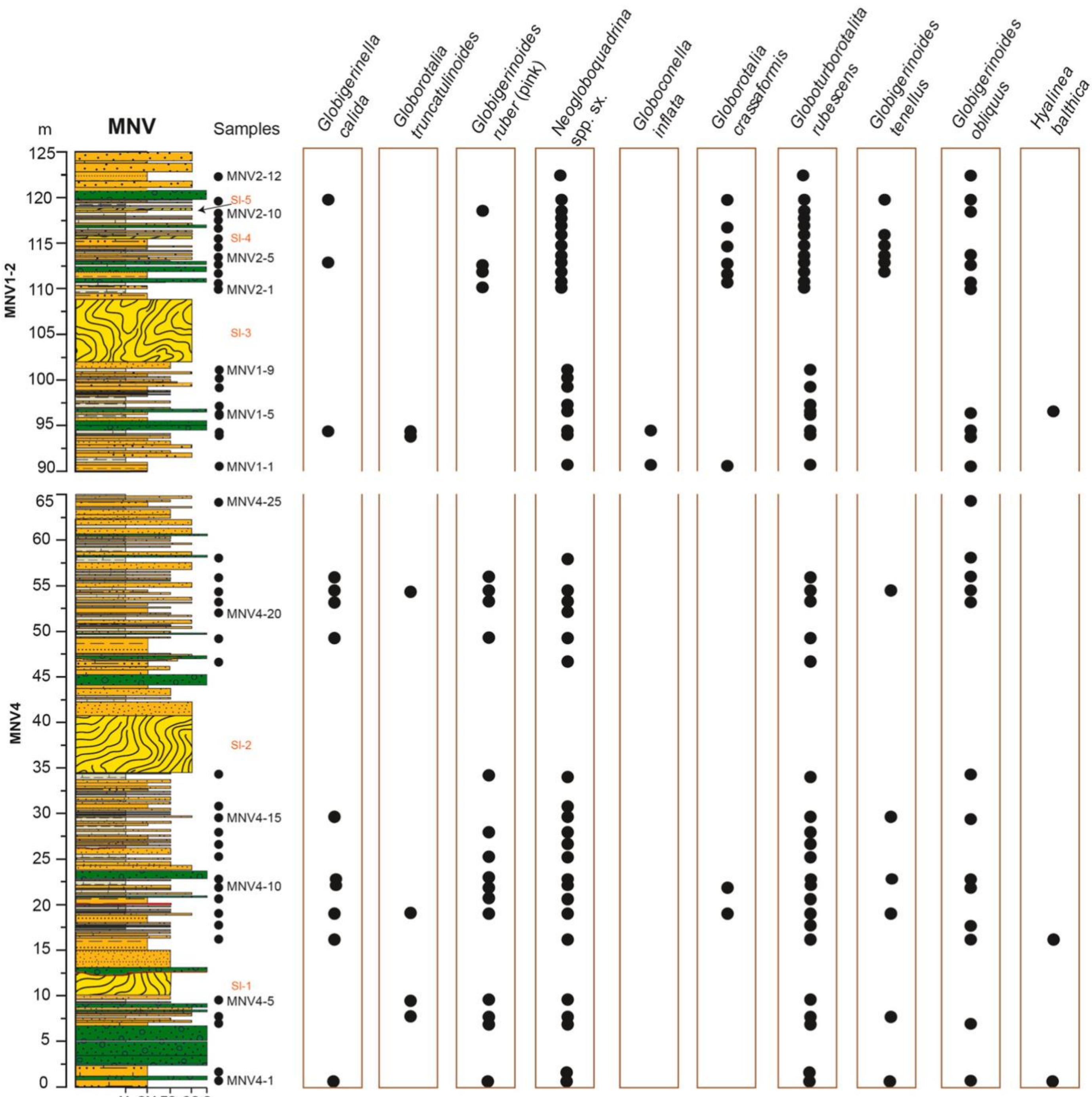

Fig. 10. Benthic and planktonic foraminifera of the MNV composite section. Dots indicate presence of each species in the corresponding sample, illustrating their vertical distribution patterns.

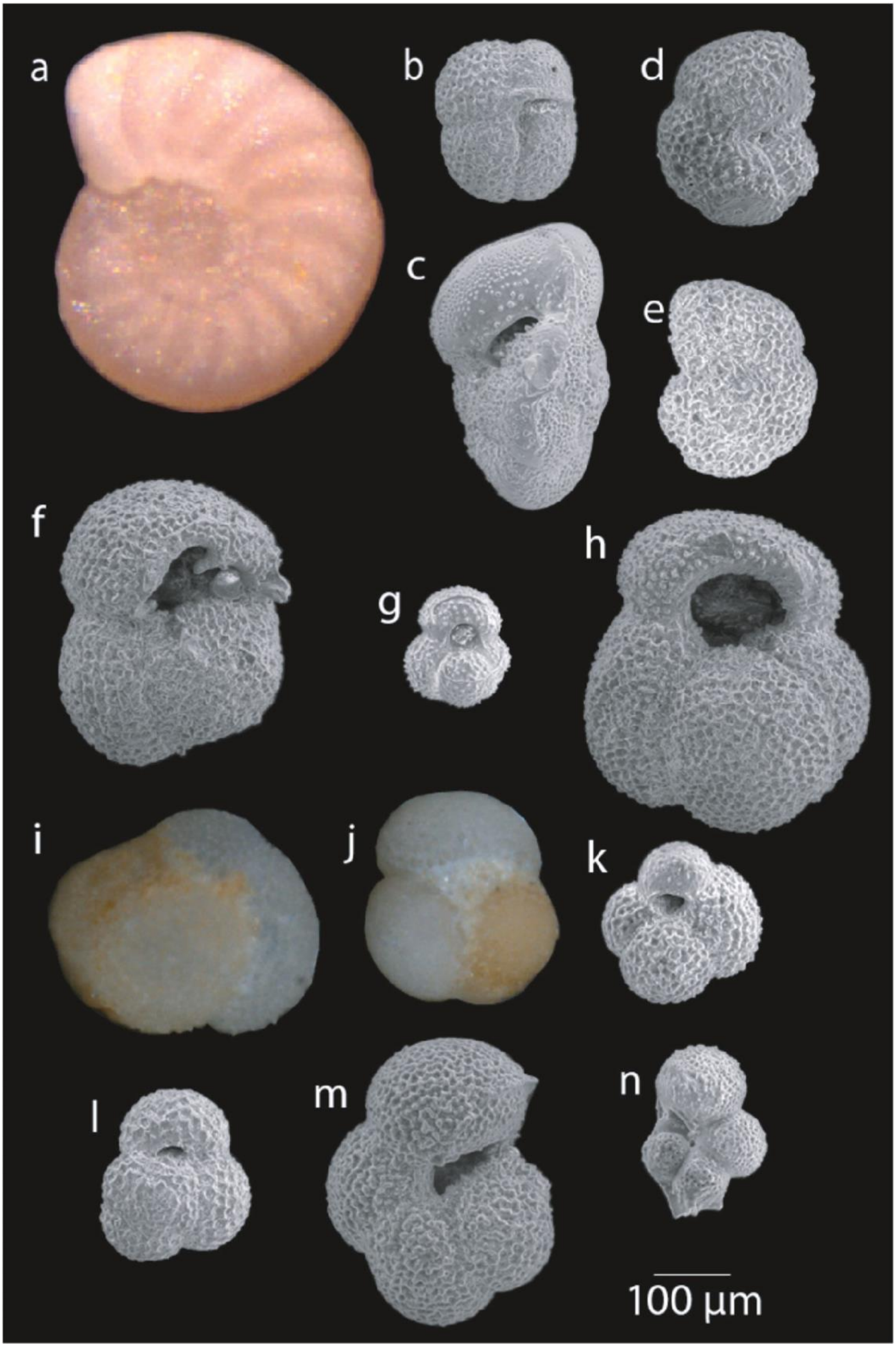

Fig. 11. SEM and optical microscope photos of foraminifer marker species. (a) *Hyalinea balthica (*umblical view) MNV4-1; (b) *Neogloboquadrina pachyderma* (umblical view) MNV4-9; (c) *Globorotalia crassaformis* (lateral view) MNV2-11; (d*) Globorotalia truncatulinoides* (umblical view) MNV3-6; (e) *G. truncatulinoides* (spiral view) MNV3-6; (f) *Globoconella inflata* (umblical view) MNV1-1; (g) *Globoturborotalita rubescens* (umblical view) MNV4-3; (h) *Globigerinoides obliquus* (umblical view) MNV4-1; (i) *Globigerinoides ruber* (pink) (umblical view) MNV4-1, j. *G. ruber* (pink) (umblical view) MNV2-10, k. *Globigerinoides tenellus* (umblical view) MNV4-22; (l) *G. tenellus* (spiral view) MNV4-15; (m) *Globigerinella calida* (umblical view) MNV4-15; (n). *Globigerinella calida* (umblical view) MNV4-19. Scale bar corresponds to 100-μm for all specimens. (For interpretation of the references to colour in this figure legend, the reader is referred to the Web version of this article.)

section (Fig. 12): 1) fan delta front; 2) fan delta front/fan prodelta.

4.1.1. Lower interval (0–24 m): fan delta front

This interval is dominated by channelized, clast-supported conglomerates, with subordinate matrix-supported conglomerates interpreted as marine debris-flow deposits. Medium-to coarse-grained sandstones are also present, along with scarce cross- and parallel-laminated sandstones indicative of low-density turbidity flows. These sandstones are interbedded with marls rich in planktonic foraminifera, reflecting vigorous sediment supply to a proximal fan delta setting. This lower interval is also characterized by the presence of a slumped horizon (2.5 m-thick) mainly consisting of matrix-supported carbonate pebbles, cobbles and boulders (rounded, sub-rounded, and angular), which show a chaotic setting with disrupted layers and minor folds. The upper part of this slumped horizon contains also angular and sub-angular grey marly boulders from the Geceleme Formation. The sedimentary structure of this slumped horizon indicates deposition by a powerful but short-lived event, like a debris-flow in the proximity of the basin margin. This slumping is affected by a synsedimentary normal fault (N150°; 60°) that presents a well-developed hangingwall clastic wedge, showing clear growth strata geometries (Fig. 13).

4.1.2. Middle interval (24–111 m): fan delta front/fan prodelta

This interval shows a marked increase in marl with abundant calcareous plankton and well-laminated fine sandstones, indicating a deeper depositional environment. Conglomerate beds, both clast- and matrix-supported, are less frequent and thinner. We interpret this facies association as transition from fan delta front to fan prodelta sedimentation, influenced by episodic turbidity flows (e.g., Wright, 1977; Coleman et al., 1998) and occasionally recording short-lived proximal marine debris flows. Two major slump complexes occur here: Sl-2, composed of thick, contorted marl–pebble masses, and Sl-3, corresponding to the paleotsunami deposit of Sagular and Özer (2024), which is exceptionally thick and extends for hundreds of meters along the outcrop, serving as a key marker for long-distance correlation.

Limestone pebbles within the slump, together with shell fragments and large clasts of bryozoan and coral colonies, suggest an extra-basial source, likely due to the erosion of the reefal limestones of the Middle Miocene Oymapınar Formation, which forms the substratum of the MNV section and characterizes the Manavgat Sub-basin margin (Flecker et al., 1998; 1998; Karabıyıkoğlu et al., 2000; İslamoglu, 2002; Çiner et al., 2008).

4.1.3. Upper interval (111–125 m): fan delta front

This interval is dominated by clast-supported conglomerates, with subordinate matrix-supported conglomerates and medium-to coarse-grained sandstones, showing coarsening- and thickening-upward trends. The interval contains also two thin slumped horizons (Sl-4 and Sl-5). The return to coarser sedimentation, with a coarsening-upward trend that includes debris flow deposits, indicates renewed fan delta progradation.

4.1.4. Depositional context

In the study section (MNV composite section), the deltaic sedimentary complex rests with an angular unconformity on the Middle Miocene shallow-water limestones of the Oymapınar Formation, as shown in the scheme of Fig. 14, revealing a significant stratigraphic gap. This gap is likely due to the complex deformation that affected the Antalya Basin from the Tortonian to the Lower Pleistocene, with phases of compression (Lycian phase, late Tortonian-early Messinian; and Aksu phase, Messinian-Zanclean) and extension (Late Pliocene-Present), which induced uplift and subsidence at the basin margin (e.g., Hall et al., 2014; Koç et al., 2016a, 2016b, 2017; McPhee et al., 2018, 2022; Wasoo et al., 2020).

In reconstructing the depositional context of the Manavgat sub-basin, it is interesting to note that the cobbles/boulders present in the different intervals of the delta complex show an inverse stratigraphy, with younger rocks in the basal interval of the delta complex (e.g., marls from the Geceleme Formation, Serravallian) and older rocks in the upper intervals (corals and bryozoan colonies from the Oymapınar Formation, Langhian). A stratigraphy with inverted clast ages often is due to tectonic uplift, basin inversion, unroofing by erosion of uplifted blocks, or recycling. In the context of the Antalya Basin, the tectonic inversion that occurred between the last compressive phase (Aksu phase, Messinian-Zanclean) and the currently ongoing extension phase (Upper Pliocene-Present) induced the uplift of the basin margin, which reversed the sediment supply.

Overall, the MNV succession records a prograding–retrograding-prograding pattern, typical of fan deltas responding to variations in basin subsidence and relative sea level. The frequent and thick slump deposits suggest rapid sediment delivery and significant basin instability.

The occurrence of synsedimentary normal faults affecting the Manavgat sedimentary succession suggests that the instability of the sedimentary basin was triggered by shaking induced by seismicity associated with the movement along those normal faults, which controlled the evolution of the delta complex within the Manavgat Sub-basin. Supporting this interpretation, Aykut et al. (2025, 2026) show U-Th and U-Pb ages of fault-related calcites indicating continuous faulting from the Middle/Late Pleistocene to the Holocene, at the transition between the subsiding Köprüçay and Manavgat sub-basins and the uplifting area of the CAP western margin.

4.2. Micropaleontological constraints of the Manavgat Sub-basin

The analysis of the micropaleontological assemblages record at the MNV succession reveals the presence of pervasive reworking, a feature typical of tectonically active fan-delta systems, where sediment is repeatedly remobilized. The succession exhibit the co-occurrence of both reworked and long-ranging species, suggesting that also many of these last are allochthonous rather than *in situ*, thereby hampering their utility as age indicators. Such taxonomic mixing likely contributed to the previously inconsistent chronological interpretations of the Manavgat Sub-basin (e.g., Akay et al., 1985; Akay and Uysal, 1988; Flecker et al., 1998; Karabıyıkoğlu et al., 2000; Deynoux et al., 2005; Çiner et al., 2008; Yılmaz et al., 2024). Despite the wide reworking, careful micropaleontological analysis enabled the identification of reliable biostratigraphic markers. The consistent presence of *Emiliania huxleyi*, whose FO in the Mediterranean is dated to approximately 0.26 Ma (Di Stefano et al., 2023), indicates that the MNV succession was deposited after ~0.26 Ma,and thus the Manavgat Sub-basin remained an active marine depocentre until the late Middle Pleistocene.

Planktonic foraminiferal assemblages complement the chronologic framework of the MNV section obtained from calcareous nannoplankton biostratigraphy, supporting the age assignment of the section to the late Middle Pleistocene. The identified species include *Globigerinoides ruber* (pink), left-coiled *Neogloboquadrina* spp., *Globigerinella calida*, and *Globorotalia truncatulinoides*, whose stratigraphic ranges extend from the Middle Pleistocene to the present.

Chronologically, the sporadic presence of *Globorotalia truncatulinoides* could indicate an age younger than 0.91 Ma, falling within the MPle2 *Globorotalia truncatulinoides excelsa* Interval Zone (Lirer et al., 2019). *Globigerinella calida* characterizes an age spanning from ~0.53 Ma to the present, and *Neogloboquadrina* spp. sx persists following the paracme end (PE), marking the reappearance of left-coiled forms at ~0.51 Ma (Lirer et al., 2019). *Globigerinoides ruber* (pink), which spans from ~0.47 Ma to the present (Numberger et al., 2009), occurs in the MNV4 and is sporadically present throughout the composite section. These taxa represent long-ranging species whose stratigraphic ranges extend to the present. Consequently, the planktonic foraminifera assemblages can only provide a maximum age of ~0.47 Ma for the Manavgat deposits.

Although the occurrence of *G. ruber* (pink) offers valuable

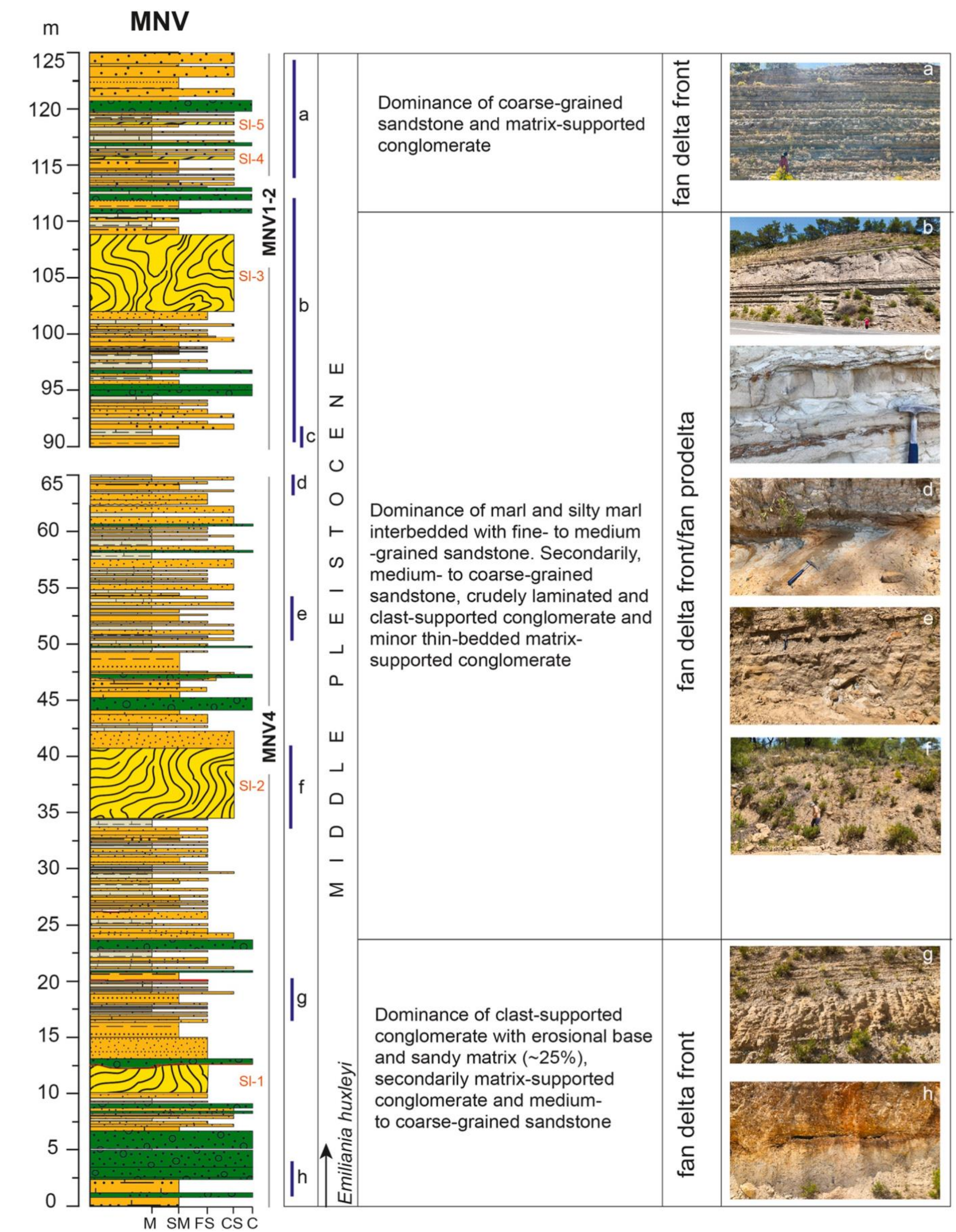

Fig. 12. Depositional environment interpretation along the Middle Pleistocene MNV composite section. To the right, some field photographs of the main lithofacies representative of the different depositional environments are shown.

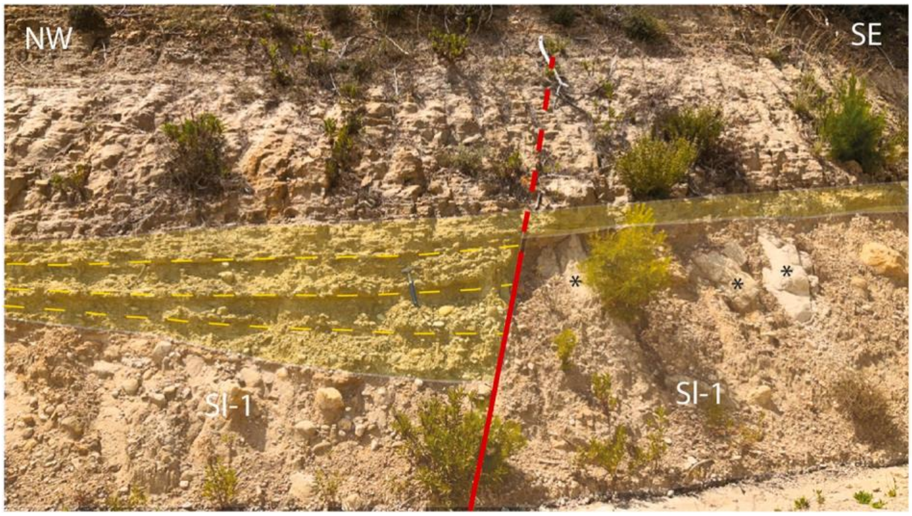

Fig. 13. Meso-scale syn-sedimentary normal fault showing a well-developed clastic-wedge, with growth-strata (yellow overlap), at the hangingwall of a fault plane (N150°, 60°) that affects the Sl-1 slumping horizon, in the basal portion of MNV4 section. Asterisks indicate some sub-angular marly boulders from the Geceleme Formation. (For interpretation of the references to colour in this figure legend, the reader is referred to the Web version of this article.)

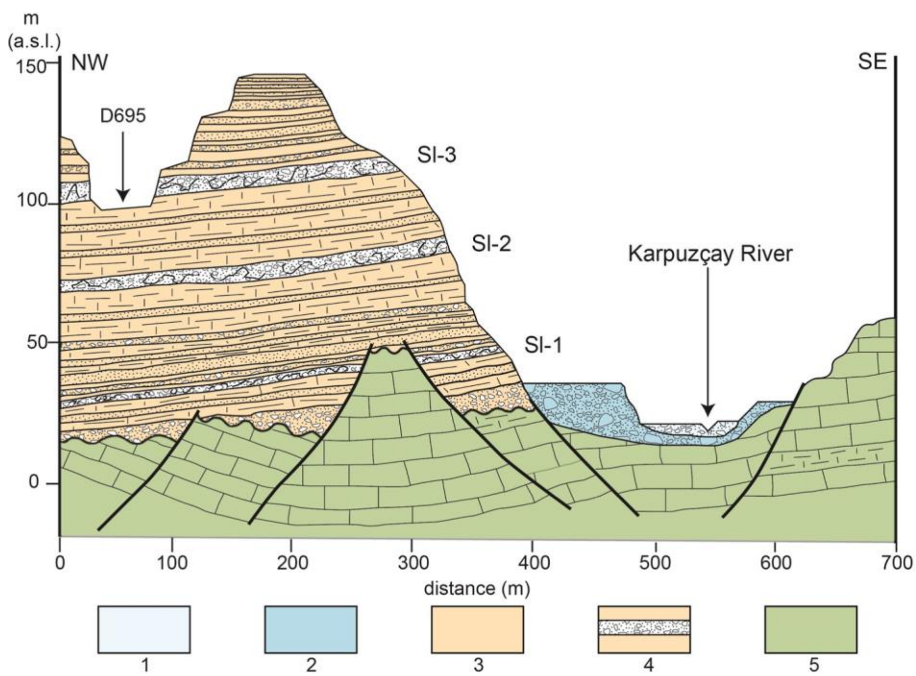

Fig. 14. Field sketch showing the relationship between the sedimentary succession of the MNV composite section (Middle Pleistocene p.p., Chibanian p.p.) and the carbonate bedrock consisting of the Oymapınar Formation, (Middle Miocene p.p., Langhian). (1) Holocene fluvial deposits; (2) Upper Pleistocene p.p. fluvial deposits; (3) marine deposits of the Manavgat Formation (Middle Pleistocene p.p.); (4) slumped horizon within the Manavgat Formation (Middle Pleistocene p.p., Chibanian); (5) shallow-water limestones of the Oymapınar Formation, (Middle Miocene p.p., Langhian). The section is exposed along the D-965 highway in the Manavgat area.

paleoenvironmental information, it should be used cautiously as a biostratigraphic marker due to regional variation in its temporal distribution. Its FO at ~0.33 Ma has been suggested by Lourens (2004) in the eastern Mediterranean Sea based on their unpublished data; however, according to Numberger et al. (2009), *G. ruber* (pink) appears as early as MIS 11 (~0.47 Ma) in the central Mediterranean Sea, and its presence is commonly associated with warm intervals (Numberger et al., 2009; Pe´rez-Folgado et al., 2004). These findings regional discrepancies likely reflect ecological and taphonomic influences rather than diachronous evolutionary events. Importantly, the presence of *G. ruber* (pink) supports the late Middle Pleistocene age yielded by the calcareous nannofossil analysis.

No ostracod specimens were recovered from the analyzed samples. This absence is consistent with deposition under high-energy, nearshore conditions, where rapid sedimentation, variable salinity, and strong hydrodynamic activity create environments unsuitable for ostracod colonization (Curtis, 1960). Such conditions reflect low environmental stability typical of shallow-marine fan-delta settings.

4.3. *Impact on the chronostratigraphy of the Antalya Basin*

Marine sedimentation within the central Isparta Angle is recorded in the Aksu, Köprüçay, and Manavgat sub-basins starting from the Early Miocene (Burdigalian), where Neogene–Quaternary sequences lie unconformably atop the Tauride carbonates (Glover and Robertson, 1998; Poisson et al., 2003a, 2003b, 2011; van Hinsbergen et al., 2010; van Hinsbergen and Schmid, 2012; Robertson et al., 2013).

The Aksu Basin preserves one of the most complete Late Cenozoic successions, comprising Miocene marine clastics with patch reefs, Pliocene shallow-marine deposits, and Lower Pleistocene–Recent marine to terrestrial clastics and travertines (Akay et al., 1985; Şengör and Yılmaz, 1981; 1996; Monod et al., 2001; Glover and Robertson, 1998; Poisson et al., 2003a, 2003b, 2011; Çiner et al., 2008; Wasoo et al., 2020). Updated foraminiferal biostratigraphy from the topmost Eskiköy Formation (Kanbur and Öğretmen, 2022) extended the age of the succession from the previously assumed Pliocene to the Early Pleistocene (1.54–1.36 Ma), based on diagnostic planktonic taxa including *Neogloboquadrina pachyderma, Globigerinoides tenellus,* and *Globoturborotalita rubescens*.

The Köprüçay Sub-basin similarly contains a mixed siliciclastic–carbonate Miocene infill, including reefal shelf carbonates, mudstones, turbidites, and thick marginal conglomerates, documented in earlier regional mapping and facies studies (Blumenthal, 1951; Flecker, 1995; Poisson et al., 2003a, 2003b; Deynoux et al., 2005; Çiner et al., 2008; Koç et al., 2016a, 2016b).

The Manavgat Sub-basin has a long history of stratigraphic investigation (Blumenthal, 1951; Bizon et al., 1974; Akay et al., 1985; Flecker, 1995, 1998, 2005; Karabıyıkoğlu et al., 2000, 2005; Deynoux et al., 2005; Çiner et al., 2008), with recent studies refining its Miocene carbonate and clastic delta facies architecture (Ilgar et al., 2024; Larsen et al., 2024a, 2024b; Wathne et al., 2024; Yılmaz et al., 2024).

Sagular and Özer (2024) proposed a significant revision of the litho- and biostratigraphy based on calcareous nannofossil assemblages. As previous authors, they placed the Oymapınar Formation (Langhian) and the overlying Geceleme Formation (Serravallian) in the Middle Miocene, but crucially, they argued that deposits of the Karpuzçay Formation, previously assigned to the Middle-Upper Miocene (Serravallian-Tortonian), in fact represent two distinct successions: (i) a Lower Pliocene clastic shelf interval, which retains the name of the Karpuzçay Formation, and (ii) a Lower Pleistocene shallow-marine unit, newly defined as the Manavgat Formation. These Lower Pleistocene strata (Manavgat Formation) are interpreted to rest unconformably on the Lower Pliocene deposits (Karpuzçay Formation) and begin with a distinctive chaotic mass-transport unit, which they attribute to a paleotsunami event. This reinterpretation extends marine sedimentation to ~1.6 Ma and reframes the stratigraphic architecture of the Manavgat Sub-basin, providing an important but debated foundation for subsequent chronostratigraphic analyses.

Our new sedimentological and micropaleontological observations provide a different perspective on both age and process. Deformed and chaotic units in the MNV composite section lack the diagnostic features of regionally sourced tsunami deposits and instead resemble internally generated slump packages typical of unstable delta settings consistent with the architecture of the MNV succession.

In particular, the mega slumping Sl-3 at the top of MNV1 corresponds to the paleotsunami event that, according to Sagular and Özer (2024), separates the Lower Pliocene deposits (Karpuzçay Formation) from those of the Lower Pleistocene (Manavgat Formation). However, in this study, Sl-3 is interpreted as an intraformational slump deposit rather than a paleotsunami. This interpretation is based on its sedimentological characteristics, including chaotic internal structure, lack of diagnostic tsunami-related features (e.g., liquefaction or tractional structures), and its consistency with downslope-directed mass-flow processes from a proximal source area.

Our results illustrate that the MNV composite section represents a continuous late Middle Pleistocene succession without hiatuses. These observations, together with the distribution of the Manavgat Sub-basin on the geological map provided by Sagular and Özer (2024), allow us to extend the Pleistocene age to the entire area that is occupied by the Karpuzçay Formation, reaching its unconformable boundary with the Geceleme Formation (Middle Miocene, Serravallian). Moreover, our results indicate that the definition of Manavgat Formation proposed by Sagular and Özer (2024) should be amended, to include the portion of the succession that these authors attributed to the Karpuzçay Formation.

This conclusion is supported by the observation that the top of the MNV composite section (~143 m above MSL) is associated with a gentle seaward dip (0.5–3°) paleosurface, defining a late Middle Pleistocene fan delta, which, extends from ~170 m (inner margin) down to ~20 m (external edge) above present sea level, elongating perpendicular to the coast over a distance from 9 to 11 km (Fig. 15).

Calcareous nannofossil evidence, together with planktonic foraminiferal assemblages, places the base of the MNV composite section, younger than ~0.26 Ma (FO of *Emiliania huxleyi*), correlating the uppermost marine deposits in the Manavgat Sub-basin with the late Middle Pleistocene (~0.23 Ma, MIS 7) strata of the TOL-1 section in the Mut Basin (Sarı et al., 2025). The presence of *E. huxleyi* at the base of the MNV section and near the top of TOL-1 demonstrates that both successions overlap within the ~0.26–0.23 Ma interval. Although the MNV record represents a higher-energy fan-delta system characterized by variable sediment accumulation, this correlation provides a strong regional chronostratigraphic anchor. Accordingly, the revised age of the MNV composite section making it nearly 1 Myr younger than the age proposed by Sagular and Özer (2024) and much younger than the previously reported marine deposits in the Antalya Basin (e.g. Karabıyıkoğlu et al., 2000, 2005; Deynoux et al., 2005; Çiner et al., 2008).

Despite extensive research across all the three sub-basins, the chronostratigraphy of the Antalya Basin remains complicated by reworking, localized hiatuses, variable sedimentation rates, and sparse high-resolution biostratigraphic control. These results refine the chronostratigraphic framework of the Manavgat Sub-basin and demonstrate that shallow-marine conditions, at least at the eastern limb of the Isparta Angle, persisted well into the late Middle Pleistocene.

4.4. Tectonic controls on the basin evolution

The Antalya Basin preserves a multi-stage tectonic history characterized by alternating phases of extension and compression throughout the Neogene–Quaternary. Regional structural, geomorphic, and paleostress datasets indicate four principal phases: (1) pre-Tortonian E–W extension gave rise to the early Antalya Basin and established the Manavgat, Köprüçay, and Aksu sub-basins (Hall et al., 2014; Koç et al., 2017; McPhee et al., 2018); (2) Tortonian–Pliocene compression, expressed by the Lycian and Aksu deformation phases along the Aksu Thrust, uplifted and folded basin strata (Glover and Robertson, 1998; Poisson et al., 2003a, 2011; Deynoux et al., 2005); (3) from the Late Pliocene onward, the region entered a renewed phase of N–S-directed extension during which inherited thrusts were reactivated as normal faults, and NW–SE-oriented fault systems, including the Kırkkavak Fault, began accommodating NE–SW extension (Glover and Robertson, 1998).

Geomorphic indicators such as deeply incised valleys, active tectonokarst depressions, and fault-controlled gorges confirm that this latest extensional regime persisted throughout the Quaternary (Üner et al., 2015; Doğan et al., 2017; Aykut et al., 2023, 2025, 2026). This prolonged extensional setting also allowed shallow-marine sedimentation to continue into the late Middle Pleistocene, as demonstrated by our new study.

Syndepositional deformation within the MNV composite section is recorded by meso-scale synsedimentary extensional faults (Fig. 13), abundant turbidity flows, and five major slump complexes (from Sl-1 to Sl-5). The disrupted internal architecture of the slump deposits and the presence of extra-basinal carbonate blocks, derived from erosion of uplifted Miocene units, indicates abrupt fault-driven slope failure, most

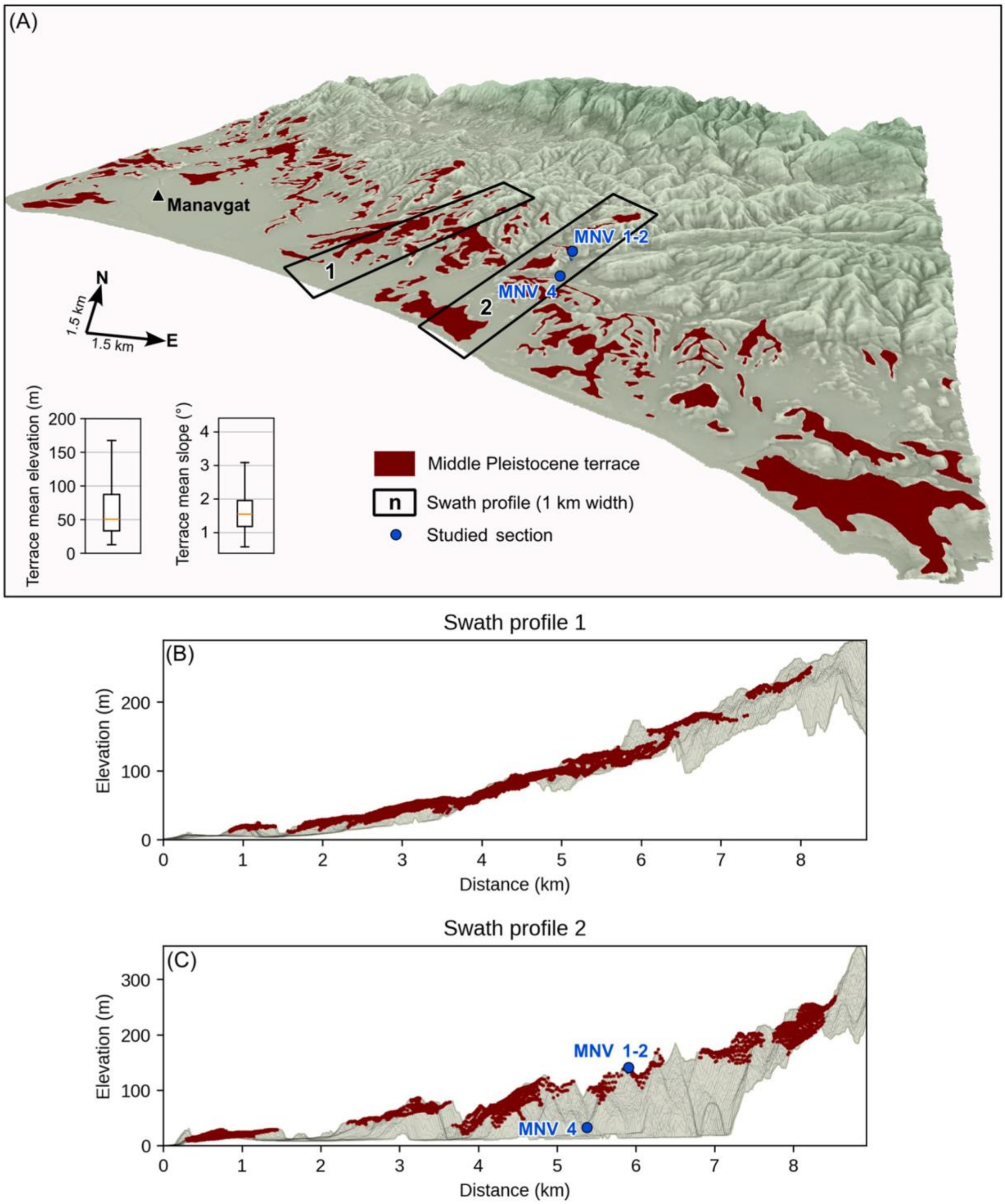

Fig. 15. (A) Three-dimensional view of the late Middle Pleistocene marine terrace identified in the Manavgat area, boxplots of the mean elevation and slope, and boxes used to trace the swath profiles. The terrace is mapped and visualized in QGIS through direct digital mapping, using the FABDEM v1.2 digital terrain model (https://data.bris.ac.uk/data/dataset/. Fare clic o toccare se si considera attendibile questo collegamento.">https://data.bris.ac.uk/data/dataset/) as base topography and red relief image map (RRM) analysis following Chiba et al. (2008); (B) Swath profile along box 1 highlithing the position of the Middle Pleistocene terrace; (C) Swath profile along box 2, highlithing the position of the Middle Pleistocene terrace and the location of the studied sections. (For interpretation of the references to colour in this figure legend, the reader is referred to the Web version of this article.)

plausibly triggered by renewed displacement along the Manavgat Basin boundary faults.

The presence of slumpings in the Middle Pleistocene succession of the Manavgat Sub-basin further links its tectono-sedimentary evolution with that of the Mut Basin, where Öğretmen et al. (2018) report a mega-slump in the Middle Pleistocene deposits at the end of the marine succession capping the CAP southern margin. These observations demonstrate that the fan-delta system of the Manavgat Sub-basin evolved in a tectonically active setting where extension, subsidence, and sediment supply interacted dynamically.

Yılmaz et al. (2024) identified two fault systems in the Manavgat Basin. Small normal faults affecting the Tepekli Formation and the larger Çardakköy Thrust, which they interpreted as placing the Karpuzçay Formation onto the Tortonian Köprüçay Conglomerate. They also proposed that early basin deepening in the east was controlled by a buried NW-trending normal fault responsible for differential subsidence across the basin (Gö̈mülü Normal Fay in Yılmaz et al., 2024). However, their tectono-stratigraphic basin evolution depends on assigning the Karpuzçay Formation a Serravallian–Tortonian age. Our revised chronostratigraphy shows that these units contain mainly late Middle Pleistocene shallow-marine deposits which requires a fundamental re-evaluation of both slip rates and timing of the tectono-sedimentary basin evolution.

After ~0.23 Ma, the basin experienced rapid uplift under continued regional extension. The correlation of the uppermost marine deposits in the MNV succession with the late Middle Pleistocene strata in the Mut Basin (~0.23 Ma, MIS 7; Sarı et al., 2025), combined with paleodepth constraints based on presence of benthic foraminifera and MIS 7 sea-level estimates (Antonioli et al., 2021), yields a mean uplift rate of ~0.8 m/kyr. This places the Manavgat Sub-basin among the most rapidly uplifting sectors of the eastern Isparta Angle.

The timing of the Manavgat Sub-basin uplift aligns with the deformation episodes at ~450 ka and 100–250 ka documented by U–Th–dated calcite veins in the western Central Anatolian Plateau (Aykut et al., 2025), indicating that uplift and extension were synchronous during the Middle Pleistocene, deeply influencing the stratigraphy of the Antalya Basin with debris flows and slumped thick horizons.

Sea level markers along the Eastern Mediterranean coast show that differential vertical motion continues into the late Holocene: the crustal block west of Antalya exhibits subsidence of —0.8 to —2.3 mm/yr (Çiner et al., 2009; Desruelles et al., 2009; Anzidei et al., 2011), whereas the Antalya–Alanya corridor shows moderate uplift of 0.17–0.35 mm/yr (Liberatore et al., 2022). This pattern is consistent with continued crustal adjustment under an extensional regime.

The underlying drivers of this Quaternary extension/uplift have been interpreted by Schildgen et al. (2012) and Howell et al. (2017), who proposed that extension reflects lithospheric warming and relaxation linked to trench-perpendicular slab tearing along the eastern margin of the Aegean slab and associated asthenosphere upwelling. In contrast, other studies attribute the extensional tectonic deformation to rollback of a remnant segment of the southern Neo-Tethyan slab (Flecker et al., 2005; Glover and Robertson, 1998; Kelling et al., 2005; Koçyiğit and Özacar, 2003; Üner et al., 2015). The most plausible interpretation is that both processes contributed: slab fragmentation and asthenosphere upwelling promoted regional uplift and crustal weakening, while continued slab rollback drove NE–SW extension and the activation of NW–SE-striking normal faults. Together, these mantle and crustal processes shaped the late Middle Pleistocene–Holocene evolution of the Manavgat Sub-basin and the whole Antalya Basin.

5. Conclusions

Integrated lithostratigraphic and micropaleontological analyses of the MNV composite section reveal a deltaic succession comprising fan delta front, fan delta front/fan prodelta, and renewed fan delta front facies, reflecting alternating high- and low-energy shallow-marine conditions. Calcareous nannofossils, together with planktic foraminiferal assemblages, constrain the base of the succession to be younger than ~0.26 Ma (FO of *Emiliania huxleyi*), while the uppermost marine deposits possibly correlate the late Middle Pleistocene strata (~0.23 Ma, MIS 7) in the Mut Basin (Sarı et al., 2025). These findings extend the age of marine deposition in the Manavgat Sub-basin well into the late Middle Pleistocene, significantly younger than previously reported (Middle Miocene or Early Pleistocene) assignments. The present elevation of the section top (~170 m above MSL), combined with paleodepth and MIS 7 sea-level reconstructions, indicates an average uplift rate of ~0.8 m/kyr since ~0.23 Ma, providing new quantitative constraints on the basin's late Quaternary tectono-sedimentary evolution. This rapid surface rise occurred under continued NE–SW-directed extension, facilitated by reactivation of the tectonic activity along NW–SE-oriented fault systems. Based on previous studies, the observed uplift/subsidence history suggests that both crustal deformation and slab-related geodynamic processes might be key drivers of the Antalya Basin's late Quaternary tectono-sedimentary evolution.

CRediT authorship contribution statement

Selma Sarı: Conceptualization, Data curation, Formal analysis, Investigation, Methodology, Visualization, Writing – original draft. **Paola Cipollari:** Conceptualization, Data curation, Investigation, Methodology, Supervision, Writing – review & editing. **Costanza Faranda:** Data curation. **Süheyla Kanbur:** Conceptualization, Data curation, Investigation, Methodology, Visualization, Writing – review & editing. **Simone Racano:** Conceptualization, Data curation, Investigation, Methodology, Visualization, Writing – review & editing. **Domenico Cosentino:** Conceptualization, Data curation, Investigation, Methodology, Supervision, Visualization, Writing – review & editing.

Declaration of competing interest

The authors declare that they have no known competing financial interests or personal relationships that could have appeared to influence the work reported in this paper.

Acknowledgements

The grant to the Department of Science of Roma Tre University (MIUR—Italy Department of Excellence, article 1, paragraph 314–337, law 232/2016) is gratefully acknowledged. The authors especially thank T.F. Schildgen, W. Nemec, and M.C. Alçiçek whose insightful comments have greatly improved our manuscript.

Data availability

Data will be made available on request.

References

Akay, E., Uysal, S., Poisson, A., Cravette, J., Müller, C., 1985. Antalya Neojen havzasinin straigrafisi. Bull. Geol. Soc. Turkey. 28, 105–119.

Akay, E., Uysal, S., 1988. Post-Eocene tectonics of the central Taurus Mountains. Bull. Min. Res. Explor. 108, 23–34.

Antonioli, F., Furlani, S., Montagna, P., Stocchi, P., 2021. The use of submerged speleothems for sea level studies in the mediterranean sea: a new perspective using glacial isostatic adjustment (GIA). Geosciences 11 (2), 77.

Anzidei, M., Antonioli, F., Benini, A., Lambeck, K., Sivan, D., Serpelloni, E., Stocchi, P., 2011. Sea level change and vertical land movements since the last two millennia along the coasts of southwestern Turkey and Israel. Quat. Int. 232 (1–2), 13–20.

Aykut, T., Uysal, I.T., Yıldırım, C., Ustaömer, T., Leonard, N., 2026. Long-term faulting history of the Central Taurides based on U-Pb dating of syn-tectonic calcites. Earth Planet Sci. Lett. 675, 119763.

Aykut, T., Yıldırım, C., Uysal, I.T., 2023. Active Deformation Pattern in the Western Flank of the Central Taurides, Southern Margin of the Central Anatolian Plateau: inferences from geomorphic markers and kinematic indicators. Tectonics 42 (6).

Aykut, T., Yıldırım, C., Uysal, I.T., Ring, U., Zhao, J.X., 2025. Coeval upper crustal extension and surface uplift in the Central Taurides (Türkiye) above the Cyprus Subduction Zone. Nat. Commun. 16 (1), 3921.

Bizon, G., Biju-Duval, B., Letouzey, J., Monod, O., Poisson, A., Özer, B., Öztümer, E., 1974. Nouvelles précisions stratigraphiques concernant les bassins tertiaires du sud de la Turquie (Antalya, Mut, Adana). Rev. Inst. Fr. Petrol 29, 305–320. Paris.

Blumenthal, M., 1951. Recherches Géologiques Dans Le Taurus Occidental Dans L'Arrière Pays D'Alanya. Mineral Research and Exploration Institute of Turkey (MTA) Publication. D5.

Bozkurt, E., 2001. Neotectonics of Turkey-a synthesis. Geodin. Acta 14, 3–30.

Chiba, T., Kaneta, S.I., Suzuki, Y., 2008. Red relief image map: new visualization method for three-dimensional data. Int. Arch. Photogramm. Remote Sens. Spatial Inf. Sci. 37 (B2), 1071–1076. https://doi.org/10.5194/isprsarchives-XXX.

Coleman, J.M., Roberts, H.H., Stone, G.W., 1998. Mississippi River delta: an overview. J. Coast Res. 14, 699–716.

Curtis, D.M., 1960. Relation of environmental energy levels and ostracod biofacies in east Mississippi delta area. AAPG Bull. 44 (4), 471–494. https://doi.org/10.1306/5D25C8B9-16C1-11D7-8645000102C1865D.

de Capoa, P., Di Donato, V., Di Staso, A., Giardino, S., Rinaldi, S., 2003. Preparation techniques and methodological approach to calcareous nannofossil analysis in silico- and calciclastic turbidites. Cour.Forsch.-Inst. Senckenberg. 244, 105–127.

Desruelles, S., Fouache, É., Çiner, A., Dalongeville, R., Pavlopoulos, K., Kosun, E., Potdevin, J.L., 2009. Beachrocks and sea level changes since Middle Holocene: comparison between the insular group of Mykonos–Delos–Rhenia (Cyclades, Greece) and the southern coast of Turkey. Glob. Planet. Chang. 66 (1–2), 19–33.

Deynoux, M., Çiner, A., Monod, O., Karabıyıkoğlu, M., Manatschal, G., Tuzcu, S., 2005. Facies architecture and depositional evolution of alluvial fan to fan delta complexes in the tectonically active Miocene Köprüçay Basin, Isparta Angle, Turkey. In: KELLING, G., ROBERTSON, A.H.F., VAN BUCHEM, F. (Eds.), Cenozoic Sedimentary Basins of South Central Turkey, 173, pp. 315–343. Sediment. Geol.

Di Stefano, A., Baldassini, N., Raffi, I., Fornaciari, E., Incarbona, A., Negri, A., Bonomo, S., Villa, G., Di Stefano, E., Rio, D., 2023. Neogene-Quaternary Mediterranean calcareous nannofossil biozonation and biochronology: a review. Stratigraphy 20 (4).

Doğan, U., Koçyiğit, A., Gökkaya, E., 2017. Development of the Kembos and Eynif structural poljes: morphotectonic evolution of the upper Manavgat River basin, Central Taurides, Turkey. Geomorphology 278, 105–120. https://doi.org/10.1016/j.geomorph.2016.10.030.

Drinia, H., Antonarakou, A., Anastasakis, G., 2014. Late Quaternary micropalaeontological record of a semi-enclosed marine basin, North Evoikos, central Aegean Sea. Quat. Int. 345, 18–31.

Dumont, J.F., Kerey, K., 1975. Basement geological study in the south of Eğirdir lake. Geol. Bull. Turk. 18 (2), 169–174.

Şengör, A.M.C., Yılmaz, Y., 1981. Tethyan evolution of Turkey: a plate tectonics approach. Tectonophysics 75 (3–4), 181–241. https://doi.org/10.1016/0040-1951(81)90275-4.

Flecker, R., 1995. Miocene Basin Evolution of the Isparta Angle, Southern Turkey. University of Edinburgh [PhD thesis].

Flecker, R., Ellam, R.M., Müller, C., Poisson, A., Robertson, A.H.F., Turner, J., 1998. Application of Sr isotope stratigraphy and sedimentary analysis to the origin and evolution of the Neogene basins in the Isparta Angle, southern Turkey. Tectonophysics 298 (1–3), 83–101.

Flecker, R., Poisson, A., Robertson, A.H.F., 2005. Facies and palaeogeographic evidence for the Miocene evolution of the Isparta Angle in its regional eastern Mediterranean context. Sediment. Geol. 173 (1–4), 277–314.

Glover, P.G., Robertson, A.H.F., 1998. Role of regional extension and uplift in the Plio–Pleistocene evolution of the Aksu Basin, SW Turkey. J. Geol. Soc. 155, 365–387.

Hall, J., Aksu, A.E., King, H., Gogacz, A., Yaltırak, C., Çifçi, G., 2014. Miocene–Recent evolution of the western Antalya Basin and its linkage with the Isparta Angle, eastern Mediterranean. Mar. Geol. 349, 1–23.

Howell, A., Jackson, J., Copley, A., McKenzie, D., Nissen, E., 2017. Subduction and vertical coastal motions in the eastern Mediterranean. Geophys. J. Int. 211 (1), 593–620. https://doi.org/10.1093/gji/ggx307.

Ilgar, A., Alçiçek, M.C., Hakyemez, A., Çiner, A., Larsen, E., Wathne, E., Nemec, W., 2024. Depositional architecture of a wave-dominated shoal-water fan delta (Manavgat Basin, southern Türkiye): implications for the Middle–Late Tortonian sea level changes and tectonics. Mediterr. Geosci. Rev. 6 (4), 421–438.

Çiner, A., Desruelles, S., Fouache, E., Kosun, E., Dalongeville, R., 2009. Beachrock formations on the Mediterranean coast of Turkey: implications for Holocene sea-level changes and tectonics. Geol. Bull. Turk. 52 (3), 257–296. https://doi.org/10.18111/gazibat.2009.52.3.257.

Çiner, A., Karabiyikoglu, M., Monod, O., Deynoux, M., Tuzcu, S., 2008. Late Cenozoic sedimentary evolution of the Antalya Basin, Southern Turkey. Turk. J. Earth Sci. 17, 1–41. https://doi.org/10.3906/yer-XXXX.

İslamoglu, Y., 2002. Antalya Miyosen Havzasının mollusk faunası ile stratigrafisi. MTA Dergisi (123–124), 27–58.

Kanbur, S., Öğretmen, N., 2022. Revised late Cenozoic foraminifer biostratigraphy of the Eskiköy Formation (Aksu Basin), SW Turkey and its paleoenvironmental conditions. Palaeogeogr. Palaeoclimatol. Palaeoecol. 591, 110883.

Karabıyıkoğlu, M., Ciner, A., Monod, O., Deynoux, M., Tuzcu, S., Orcen, S., 2000. Tectonosedimentary evolution of the Miocene Manavgat Basin, western Taurides, Turkey. In: Bozkurt, E., Winchester, J.A., Piper, J.D.A. (Eds.), Tectonics and Magmatism in Turkey and the Surrounding Area, 173. Geol. Soc. Lond. Spec. Publ, pp. 271–294. https://doi.org/10.1144/GSL.SP.2000.173.01.14.

Kelling, G., Robertson, A.H.F., Buchem, F.V., 2005. Cenozoic sedimentary basins of southern Turkey: an introduction. Sediment. Geol. 173, 1–13.

Koç, A., Kaymakci, N., Van Hinsbergen, D.J.J., Kuiper, K.F., 2017. Miocene tectonic history of the Central Tauride intramontane basins, and the paleogeographic evolution of the Central Anatolian Plateau. Glob. Planet. Change. 158, 83–102. https://doi.org/10.1016/j.gloplacha.2017.09.001.

Koç, A., Kaymakci, N., Van Hinsbergen, D.J.J., Vissers, R.L.M., 2016a. A Miocene onset of the modern extensional regime in the Isparta Angle: constraints from the Yalvaç Basin (southwest Turkey). Int. J. Earth Sci. 105, 369–398.

Koç, A., van Hinsbergen, D.J.J., Kaymakci, N., Langereis, C.G., 2016b. Late Neogene oroclinal bending in the central taurides: a record of terminal eastward subduction in southern Turkey? Earth Planet Sci. Lett. 434, 75–90. https://doi.org/10.1016/J.EPSL.2015.11.020.

Koçyiğit, A., Doğan, U., Gürboğa, Ş., Kalafat, D., 2024. Quaternary tensional neotectonics of the southwestern flank of the Isparta Angle, Antalya, Türkiye. Medit. Geosc. Rev. 6 (4), 589–613.

Koçyiğit, A., Ozacar, A., 2003. Extensional neotectonic regime through the NE edge of the outer Isparta Angle, SW Turkey: new field and seismic data. Turk. J. Earth Sci. 12 (1), 67–90.

Larsen, E., Nemec, W., Alçiçek, M.C., Helland, O.M., 2024a. The Göktaş fan delta complex in Manavgat Basin, South Türkiye: a model for stratigraphic development of coarse-clastic littoral wedges and spatial-facies prediction. Medit. Geosc. Rev. 6 (4), 363–395.

Larsen, E., Nemec, W., Ellingsen, T.R., 2024b. The frontal facies and sedimentation processes of a shoal-water fan delta in the Köprü Basin of southern Türkiye. Medit. Geosc. Rev. 6 (4), 303–337.

Liberatore, M., Gliozzi, E., Cipollari, P., Öğretmen, N., Spada, G., Cosentino, D., 2022. Vertical velocity fields along the Eastern Mediterranean coast as revealed by late Holocene sea-level markers. Earth Sci. Rev. 234, 104199. https://doi.org/10.1016/j.earscirev.2022.104199.

Lirer, F., Foresi, L.M., Iaccarino, S.M., Salvatorini, G., Turco, E., Cosentino, C., Sierro, F.J., Caruso, A., 2019. Mediterranean Neogene planktonic foraminifer biozonation and biochronology. Earth Sci. Rev. 196, 102869.

Lourens, L.J., 2004. Revised tuning of Ocean Drilling Program Site 964 and KC01B (Mediterranean) and implications for the δ18O, tephra, calcareous nannofossil, and geomagnetic reversal chronologies of the past 1.1 Myr. Paleoceanography 19 (3).

McPhee, P.J., Altıner, D., van Hinsbergen, D.J.J., 2018. First balanced cross section across the Taurides fold-thrust belt: geological constraints on the subduction history of the Antalya slab in southern Anatolia. Tectonics 37 (10), 3738–3759. https://doi.org/10.1029/2017TC004893.

McPhee, P.J., Koç, A., van Hinsbergen, D.J.J., 2022. Preparing the ground for plateau growth: late Neogene Central Anatolian uplift in the context of orogenic and geodynamic evolution since the Cretaceous. Tectonophysics 822, 229131. https://doi.org/10.1016/j.tecto.2021.229131.

Monod, O., Kuzucuoglu, C., Okay, A., 2006. A Miocene palaeovalley network in the Western Taurus (Turkey). Turk. J. Earth Sci. 15, 1–23.

Monod, O., Manatschal, G., Deynoux, M., Ciner, A., Karabiyikoglu, M., Tuzcu, S., Kuzucuoglu, C., 2001. Neogene morphotectonics in the Köprü Basin (Isparta Angle, Southern Turkey). Terra Nova 13, 524 (Abstract).

Nemec, W., Alçiçek, M.C., Özaksoy, V., 2018. Sedimentation in a foreland basin within synorogenic orocline: palaeogene of the Isparta Bend, Taurides, SW Turkey. Basin Res. 30 (4), 650–670.

Üner, S., Özsayin, E., Kutluay, A., Dirik, K., 2015. Polyphase tectonic evolution of the Aksu Basin, Isparta Angle (Southern Turkey). Geol. Carpath 66 (2), 157–169. https://doi.org/10.1515/geoca-2015-0017.

Numberger, L., Hemleben, C., Hoffmann, R., Mackensen, A., Schulz, H., Wunderlich, J.M., Kucera, M., 2009. Habitats, abundance patterns and isotopic signals of morphotypes of the planktonic foraminifer Globigerinoides ruber (d'Orbigny) in the eastern Mediterranean Sea since the Marine Isotopic Stage 12. Mar. Micropaleontol. 73 (1–2), 90–104.

Okay, A.I., Zattin, M., Cavazza, W., 2010. Apatite fission-track data for the Miocene Arabia-Eurasia collision. Geology 38 (1), 35–38. https://doi.org/10.1130/g30234.1.

Parlak, O., Dunkl, I., Karaoğlan, F., Kusky, T.M., Zhang, C., Wang, L., Koepke, J., Billor, Z., Hames, W.E., Şimşek, E., Şimşek, G., 2019. Rapid cooling history of a Neotethyan ophiolite: evidence for contemporaneous subduction initiation and metamorphic sole formation. GSA Bulletin 131 (11–12), 2011–2038.

Poisson, A., Orszag-Sperber, F., Kosun, E., Bassetti, M.A., Müller, C., Wernli, R., Rouchy, J.M., 2011. The Late Cenozoic evolution of the Aksu basin (Isparta Angle; SW Turkey). New insights. Bull. Soc. Geol. Fr. 182 (2), 133–148.

Poisson, A., Wernli, R., Sagular, E.K., Temiz, H., 2003b. New data concerning the age of the Aksu Thrust in the south of the Aksu Valley, Isparta Angle (SW Turkey): consequences for the Antalya Basin and the eastern Mediterranean. Geol. J. 38, 311–327.

Poisson, A., Yağmurlu, F., Bozcu, M., Fientürk, M., 2003a. New insights on the tectonic setting and evolution around the apex of the Isparta Angle (SW Turkey). Geol. J. 38, 257–282.

Pérez-Folgado, M., Sierro, F.J., Flores, J.A., Grimalt, J.O., Zahn, R., 2004. Paleoclimatic variations in foraminifer assemblages from the Alboran Sea (Western Mediterranean) during the last 150 ka in ODP Site 977. Mar. Geol. 212 (1–4), 113–131.

Öğretmen, N., Cipollari, P., Frezza, V., Faranda, C., Karanika, K., et al., 2018. Evidence for 1.5 km of uplift of the Central Anatolian Plateau's southern margin in the last 450 kyr and implications for its multiphased uplift history. Tectonics 37 (1), 359–390. https://doi.org/10.1002/2017TC004805.

Robertson, A.H., Parlak, O., Ustaomer, T., 2013. Late Palaeozoic–Early Cenozoic Tectonic Development of Southern Turkey and the Easternmost Mediterranean Region: Evidence from the Inter-relations of Continental and Oceanic Units, 372. Geol. Soc. Lond. Spec. Publ, pp. 1–35. https://doi.org/10.1144/SP372.4.

Sagular, E.K., Özer, G.Y., 2024. Chrono-biostratigraphic analysis of the Lower Pleistocene paleotsunami deposits overlying the Late Pliocene Erosional Surface (LPES) at the Manavgat Subbasin (SW Türkiye) based on new nannofossil and fossil ascidian spicule data. Geosound 60, 38–82.

Sarı, S., Cipollari, P., Cosentino, D., Gliozzi, E., Lirer, F., Kanbur, S., Ogretmen, N., Mattei, M., Cifelli, F., Faranda, C., 2025. The Middle Pleistocene uplift of the Central Anatolian Plateau (CAP) southern margin: new evidence from the Mut Basin (South Turkey). In: EGU General Assembly 2025, Vienna, Austria. https://doi.org/10.5194/egusphere-egu25-10350. EGU25-10350.

Schildgen, T.F., Cosentino, D., Caruso, A., Buchwaldt, R., Yildirim, C., Bowring, S.A., 2012. Surface expression of eastern Mediterranean slab dynamics: neogene topographic and structural evolution of the southwest margin of the Central Anatolian Plateau, Turkey. Tectonics 31 (2). https://doi.org/10.1029/2011TC003021.

Schmid, T.C., Schreurs, G., Adam, J., 2022. Characteristics of continental rifting in rotational systems: new findings from spatiotemporal high resolution quantified crustal scale analogue models. Tectonophysics 822, 229174, 10-1016.

Tiryakioğlu, İ., Floyd, M., Erdoğan, S., Gülal, E., Ergintav, S., McClusky, S., Reilinger, R., 2013. GPS constraints on active deformation in the Isparta Angle region of SW Turkey. Geophys. J. Int. 195 (3), 1455–1463.
van Hinsbergen, D.J., Dekkers, M.J., Koç, A., 2010. Testing Miocene remagnetization of Bey Dağları: timing and amount of Neogene rotations in SW Turkey. Turk. J. Earth Sci. 19 (2), 123–156.
van Hinsbergen, D.J., Schmid, S.M., 2012. Map view restoration of Aegean–West Anatolian accretion and extension since the Eocene. Tectonics 31 (5).
Över, S., Özden, S., Kamacı, Z., Yılmaz, H., Ünlügenç, U.C., Pınar, A., 2016. Upper crust response to geodynamic processes beneath Isparta Angle, SW Turkey: revealed by CMT solutions of earthquakes. Tectonophysics 687, 94–104.
Wasoo, M.H., Özkaptan, M., Koç, A., 2020. New insights on the Neogene tectonic evolution of the Aksu Basin (SE Turkey) from the Anisotropy of Magnetic Susceptibility (AMS) and paleostress data. J. Struct. Geol. 139, 104–137.
Wathne, E., Larsen, E., Nemec, W., Alçiçek, M.C., Ilgar, A., Helland, O.M., 2024. The Katırınemeği and Asar fan delta complexes in the Manavgat Basin (southern Türkiye): facies architecture of small shoal-water deltas recording forced and normal regressions. Mediterr. Geosci. Rev. 6 (4), 397–420.
Wright, L.D., 1977. Sediment transport and deposition at river mouths: a synthesis. GSA Bulletin 88 (6), 857–868.
Yılmaz, Y.E., Atakul-Ozdemir, A., Koc, A., 2024. Manavgat Havzasının (Antalya, Türkiye) Neojen litostratigrafisi ve yapısal unsurları. Geol. Bull. Turk. 67 (1), 71–114.
Özgül, N., 1976. Torosların bazı temel jeoloji özellikleri. Geol. Bull. Turk. 19, 65–78.